A STUDY ON THE EFFECTS OF A MAGNETIC FIELD ON THE CORROSION BEHAVIOR OF MATERIALS

by

SOUNDARYA PONDICHERY

Presented to the Faculty of the Graduate School of

The University of Texas at Arlington in Partial Fulfillment

of the Requirements

for the Degree of

MASTER OF SCIENCE IN MATERIALS SCIENCE AND ENGINEERING

THE UNIVERSITY OF TEXAS AT ARLINGTON

December 2014

Acknowledgements

I would like to sincerely thank Dr. Efstathios I. Meletis, for his guidance, instructions and encouragement throughout the research project work. I would like to thank Dr. Wetz for providing me some guidance during the beginning of this project. I would like to thank Dr. Tibbals and Dr. Jiang for serving on my committee.

I'd like to acknowledge the UTA laboratories SaNEL and CCMB, for having efficient facilities that made this research a success.

I would like to acknowledge my group members for their support. I would specially like to thank Tapas Desai for training me and guiding me with this project. I would like to thank Adam Smith for his assistance with the Nano-Indenter and Randall Kelton for help on designing the experimental set-up. I would also like to thank Clint Gnengy-Davidson for co-cordially working with me during my initial project designing and set-up.

Finally, I would like to thank my family for their cooperation and support throughout my studies.

November 19, 2014

Abstract

A STUDY ON THE EFFECTS OF MAGNETIC FIELD ON

THE CORROSION BEHAVIOR OF MATERIALS

Soundarya Pondichery, M.S.

The University of Texas at Arlington, 2014

Supervising Professor: Efstathios I. Meletis

Corrosion can cause deterioration of a material due to its interaction with the environment. Corrosion control is being one of the biggest challenges in most industries. There are various notable and unknown factors that influence the rate of corrosion of a certain material/environment system. Magnetic fields and their effects on electrochemical reactions have recently gained significant interest. Various magnetic field driven forces occurring in an electrolyte have been reported during an electrochemical reaction. Lorentz force driven convection in the electrolyte, known as MHD (Magnetohydrodynamics) effect and paramagnetic gradient forces are reported to be the most effective.

This research studies the effects of an external magnetic field on the electrochemical nature of materials in 3.5% NaCl solution. To understand and analyze magnetic field effects on a wide range of materials, both ferromagnetic and non-magnetic materials which are active and active-passive type are studied

in near sea water solution, i.e. 3.5% NaCl solution. Potentiodynamic polarization and corrosion potential vs time tests were carried out to study and analyze the corrosion behavior. Corrosion testing results were obtained both with and without the influence of an external magnetic field of 0.75T. On comparing the electrochemical behavior results of both conditions, it clearly depicts the effect of an external magnetic field on the corrosion potential and corrosion rate. In the case of ferromagnetic materials like 416 stainless steel (SS) and 1018 carbon steel, a cathodic shift of the corrosion potential and increase in the corrosion rate was observed. While for ferrous but non-magnetic and passivating material like 304 SS, no effect of the magnetic field was observed which can be attributed to its non-magnetic austenitic phase and highly stable oxide formation tendency. Also, no effect was observed on the non-ferrous alloys like Ti alloy (Ti6Al4V) and pure Zn. Due to diamagnetic nature of its ions but also of its actively passivating behavior, Ti presented no effect by the magnetic field. Pure Zn also did not exhibited magnetic field effects but basically due to its already strong activation polarization behavior. Scanning electron micrographs of the surface morphology after corrosion testing were consistent with the electrochemical findings. They confirmed the increased corrosion activity on 416 SS and 1018 carbon steel with no effect on 304 SS, Ti alloy and pure Zn.

Table of Contents

Acknowledgement.....iii

Abstract.....iv

List of Figures viii

List of Tables xi

Chapter 1 INTRODUCTION..... 1

Chapter 2 OBJECTIVE 5

Chapter 3 LITERATURE REVIEW..... 7

3.1 Introduction to the Electrochemistry of Corrosion 7

3.2 Basic Process and Kinetics of Corrosion 9

3.3 Types of Corrosion..... 13

3.4 Electrochemical Nature of Metals..... 15

3.3 Magnetic Field Effect on Corrosion Behavior 21

3.3.1 Magnetic field effect on anodic behavior of ferromagnetic materials ..25

3.3.2 Magnetic Field effects on corrosion behavior of non-ferrous alloy.....32

Chapter 4 EXPERIMENTAL 35

4.1 Materials..... 35

4.1.1 Materials Selection *35*

4.1.2 Permanent Magnet.....*38*

4.1.3 Electrolyte 38
4.2 Electrochemical Testing..... 38
4.2.1 Electrochemical Cell for baseline experiments.....38
4.2.2 Electrochemical Cell for Magnetic field influenced experiments.....40
4.2.3 Electrochemical Testing.....41
4.3 Characterization 44
4.3.1 X-Ray Diffraction.....44
4.3.2 Scanning Electron Microscopy (SEM) and Energy dispersive Electron Spectroscopy (EDS) 45
Chapter 5 RESULTS AND DISCUSSION 47
5.1 X-Ray Diffraction analysis..... 47
5.2 Electrochemical Testing..... 48
5.2.1 Corrosion Behavior of Ferrous Alloys 50
Chapter 6 CONCLUSIONS..... 72
References..... 74
Biographical Information..... 83

List of Figures

Figure 1-1: GE gas turbines power U.S. Navy electrical propulsion system [2].....3

Figure 3-1: Variations of anodic behavior of passivating metals seen in aqueous solutions [13].....12

Figure 3-2: Metal/metal ion reversible potentials in relation to the cathodic polarization curve for oxygen reduction [12].....17

Figure 3-3: Schematic of polarization curves for corrosion, passivation and passive film breakdown for stainless steels in dilute acid solutions [12].....19

Figure 3-4: Simplified potential-pH diagram for iron in a solution containing dissolved iron at a concentration of 10^{-6} M at temperature 25°C [12].....21

Figure 3-5: Schematically representation of induced Lorentz force in the presence of mutually perpendicular magnetic and electrical fields [2].....23

Figure 3-6: The potentiodynamic curves of iron in phthalate buffer (pH 5) without and with magnetic field applied (a) parallel and (b) perpendicular to the electrode surface (scan rate of 0.5mV/s) [72].....27

Figure 3-7: The potentiodynamic curves of iron in phthalate buffer (pH 5) without and with magnetic field applied (a) parallel and (b) perpendicular to the electrode surface (scan rate of 0.5mV/s) [72].....31

Figure 4-1 Sample as after preparation (with mirror finish).....37

Figure 4-2: K0047 Corrosion cell from Princeton Applied Research.....40

Figure 4-3: Electrochemical Cell with a NdFeN50 permanent magnet in the holder, attached alongside the cell.....41
Figure 4-4: Electrochemical Testing experimental set-up available at SaNEL.....43
Figure 4-5: X-Ray Diffraction method to measure the intensity diffracted from the hkl planes at an angle Ψ to the surface of the specimen [103].....45
Figure 5-1: X-Ray Diffraction pattern of 304 stainless steel.....48
Figure 5-2: Comparison of results of (a) Corrosion potential Vs time measurement and (b) Potentiodynamic polarization curves of 304 SS in 3.5% NaCl, both without and with an external magnetic field.....51
Figure 5-3: SEM micrographs of 304 SS in 3.5% NaCl solution (a) without and (b) with impact of an external magnetic field.....54
Figure 5-4: Comparison of results of (a) Corrosion potential Vs time measurement and (b) Potentiodynamic polarization curves of 416 SS in 3.5% NaCl, both without and with an external magnetic field.....58
Figure 5-5: SEM micrographs of 416 SS in 3.5% NaCl solution (a) without a magnetic field and (b) with impact of an external magnetic field (both at edge and center).....61
Figure 5-6: Comparison of results of (a) Corrosion potential Vs time measurement and (b) Potentiodynamic polarization curves of 1018 steel in 3.5% NaCl, both without and with an external magnetic field.....64

Figure 5-7: Comparison of results of (a) Corrosion potential Vs time measurement and (b) Potentiodynamic polarization curves of Zn in 3.5% NaCl, both without and with an external magnetic field.....67
Figure 5-8: Comparison of results of (a) Corrosion potential Vs time measurement and (b) Potentiodynamic polarization curves of Ti alloy in 3.5% NaCl, both without and with an external magnetic field.....70

List of Tables

Table 3-1: Various types of corrosion based on the system and driving force [2].....14

Table 4-1**:** Nominal elemental composition of 304 SS, 416 SS and 1018 Low-carbon Steel.....36

Table 5-1: Potentiodynamic polarization curves report of 304 SS in 3.5% NaCl solution with and without an external magnetic field.....52

Table 5-2: Potentiodynamic polarization curves report of 416 SS in 3.5% NaCl solution with and without an external magnetic field.....59

Table 5-3: Potentiodynamic polarization curves report of 1018 steel in 3.5% NaCl solution with and without an external magnetic field.....65

Table 5-4: Potentiodynamic polarization curves report of Zn in 3.5% NaCl solution with and without an external magnetic field.....68

Table 5-5: Potentiodynamic polarization curves report of Ti alloy in 3.5% NaCl solution with and without an external magnetic field.....71

Chapter 1

INTRODUCTION

Corrosion is an electrochemical phenomenon of material degradation (most commonly metals/alloys) due to its environment. The environment acts like the electrolyte of the corrosion cell and the concentration, constituents and relative motion of electrolyte are some of the common factors that influence the rate of corrosion [1]. Corrosion has tremendous effects on all large and small scale industries which are a part of our economy, ranging from electronics to transportation industries. It is estimated that about 150 million tons of steel are destroyed per year due to corrosion that corresponds to one quarter of the world's annual steel production [1]. Due to corrosion's annual cost worldwide of $2.2 trillion dollars, governments and structural industries are looking into reducing replacement and maintenance costs by understanding the corrosion process and protecting the alloys used. Corrosion of steel structures in marine environments is a major concern which has to be considered during the design and maintenance, by the US Naval industry [2].

US Naval Research Lab is carrying out broad scientific and research programs to predict and control the marine environment effects on the corrosion of naval systems. The most recent efforts of the research programs involve the study of the effect of high magnetic fields on the corrosion behavior of the naval

structures. In the near future, the US Navy plans to integrate more electrical propulsions and electrical architectures in its fleet. These integrations will require incorporation of new electrical architectures which will operate at high voltage levels of several kilo-volts (kV), and high current of few Mega-amps (MA). The power systems deliver low to moderate currents to few loads in a continuous mode of operation while other loads are delivered high currents in a pulsed mode of operation. Due to variation in operating high currents, high magnetic fields are generated which will be spread not only within the current carrying conductor but also throughout the proximity of the current carrying conductor. Most likely, primary conductors which carry current to the loads are copper and aluminum while other metals/ alloys of steel, nickel, and titanium are used for other structural applications in and around the electrical assemblies. These metallic and alloy components are exposed to the high magnetic fields generated. Since most of the electrical components carry high currents which intersect the high magnetic field lines and produces an electromagnetic force.

Figure 1-1: GE gas turbines power U.S. Navy electric propulsion system [2]

Magnetic fields can affect electrochemical reactions, especially mass transport rates, for metallic materials in aqueous solutions [3-6]. Some considerable research has also been performed on the effects of magnetic fields on the electron transfer process in electrode-solution systems [7-10]. The main effect of a magnetic field applied on an electrochemical system is the introduction of additional forces on the ions in the electrolyte [11]. Lorentz force is the most generally accepted. Lorentz force, paramagnetic gradient force, forces driven convection are the most recently studied and documented research in respect to

effects of magnetic field on the electrochemical behavior of metals and their alloys.

Therefore, when a material is influenced by a magnetic field and is subjected to an aggressive environment, an effect on its corrosion rate can be expected when compared to its corrosion rate when not influenced by the magnetic field. By the support of previous research, a more positive or negative shift in the corrosion potential may also be expected when comparing that under the influence of a magnetic field and that in a magnetic field-free environment. This thesis is to study, analyze and understand this effect on judiciously selected types of materials.

Chapter 2

OBJECTIVE

One main objective of this research is to give relevant information on the possible effect of magnetic field on the corrosion behavior of metals in similar environments. Though various metals and their alloys are subjected to similar type of aggressive environments, they behave in different manner. For electrical and mechanical-electric propulsions, electromagnet power generators and electrical capsulations a wide range of metals and metallic alloys are used. Most commonly used are stainless steel, aluminum, nickel and copper alloys. These alloys are exposed to high magnetic fields directly or indirectly during power generation and other applications. Considering the adverse and most severe situation, which these metallic components can be exposed to, this research is a study on their corrosion behavior in such environments.

This thesis in conducted to clearly understand magnetic field effects on the anodic dissolution, passivation and trans passivation behavior of both ferrous and non-ferrous metals in 3.5% NaCl solution (near sea water composition). To do so, a variety of metals were selected which have different combinations of electrochemical and magnetic nature that include magnetic, non-magnetic, active dissolution and active passivation. Hence, the study of the corrosion behavior of 304 stainless steel (SS), 416 SS, 1018 Steel, titanium alloy (Ti 6Al4V) and zinc

(pure Zn) under the influence of an external magnetic field, is the primary objective of this research study.

Chapter 3

LITERATURE REVIEW

Corrosion has always been one of the major concerns of most industries. By the evolution of modern technology and integration of highly complicated systems, the challenges to be faced are also rapidly increasing. Where, corrosion has been one predominant cause for failure, material loss and inefficiency in different sections of these modern developments. Various researchers are making efforts to eradicate or at least minimize this phenomenon. The concern of corrosion exists for a wide range of sectors; from nanoscale level in NEMS and MEMS to macro scale level in heat exchangers and boilers, from extreme cold to hot conditions as well as ambient conditions over time. Hence, the study of corrosion is most emphasized on various factors affecting it and the kinetics of this process.

3.1 Introduction to the Electrochemistry of Corrosion

Corrosion is an irreversible electrochemical process that results in the loss of material, by dissolution due to its environment. Its environment acts like an electrolyte and any changes in the nature of the electrolyte greatly affects the kinetics of corrosion phenomena. It is a process that involves exchange of ions and electrons between an anode and cathode, through the electrolyte which occurs due to a potential difference that is present at the material/environment interface.

The anodic material undergoes dissolution and loss of electrons and hence gets oxidized. The oxidation of the metallic surface involves electrochemical reactions and other factors that control its kinetics.

In nature, all metal surfaces (except gold) are covered with its own oxide films when exposed to air. When the metal gets in contact to an aqueous environment, it breaks down the oxide film. If exposed to an acidic solution, complete dissolution of oxide film will occur and leave behind a bare metal surface which can further be degraded. While when exposed to near neutral solutions, the extent of oxide layer degradation will tend to be smaller since the solubility of the oxide layer is much lower. In such cases, the initial breakdown of metallic oxide layer occurs at areas of some discontinuity in the metal structure, e.g. at defects such as grain boundaries or presence of inclusions. The oxide layer thickness decreases or may be more prone to dissolution at defect areas than elsewhere. In cases where there are inhibiting anions present in the near-neutral solution, dissolution of the oxide layer is suppressed and oxide film is stabilized to form a passivating oxide film which can efficiently inhibit the metal from corrosion, is then in the passive state [12].

3.2 Basic Process and Kinetics of Corrosion

The basic process of metallic corrosion in an aqueous solution consists of the anodic dissolution of metals and the cathodic reduction of oxidants present in the solution. The chemical representation of the reaction is:

Anodic reaction involved in the electrochemical test:

$$M \rightarrow M^{n+} + ne^- \quad (1)$$

Five possible cathodic reduction reactions:

$$2\,H_2O + 2\,e^- \rightarrow H_{2(g)} + 2\,OH^-_{(aq)} \quad E^o_{red} = -0.632 \text{ V vs. SCE} \quad (2)$$

$$2\,H^+ + 2\,e^- \rightarrow H_{2(g)} \quad E^o_{red} = -0.192 \text{ V vs. SCE} \quad (3)$$

$$O_{2(g)} + 2\,H_2O + 4\,e^- \rightarrow 4\,OH^-_{(aq)} \quad E^o_{red} = +0.628 \text{ V vs. SCE} \quad (4)$$

$$O_{2(g)} + 4\,H^+ + 4\,e^- \rightarrow 2\,H_2O \quad E^o_{red} = 1.038 \text{ V vs. SCE} \quad (5)$$

$$M^{n+} + ne^- \rightarrow M \quad (6)$$

Since the redox reactions (Eqs. 1-6) involve the transfer of electrons and ions between the metal and the solution the rates are equivalent to electric currents. The rates of these electrochemical reactions depend on the potential difference between the metal and the electrolytic solution, i.e. the instantaneous potential of the metal electrode in that particular solution. The potential of a metallic corroding electrode in aqueous solution is known as the corrosion potential. It is relative to its aqueous solution and lies in the range between the

equilibrium potential of anodic oxidation and cathodic reduction. It is known from the corrosion kinetics, that the anodic oxidation current of metal degradation and the cathodic reduction current of the oxidant are equal, at the corrosion potential. When the metal electrode potential is more positive, the rates of cathodic reactions increase and the rates of anodic reactions decrease accordingly. Conversely, as the metal electrode potential becomes more negative, the effect on the reactions is opposite. The relationships between the potential of a metal and the currents flowing (which is equivalent to the rates of corrosion reactions), in the electrochemical system, can be used to study the corrosion behavior of the metal in that system. Relation between potential and current in the electrochemical system is used to determine the corrosion kinetics. These curves are plotted by electrode potential versus the reaction current for both anodic oxidation and cathodic reduction and are known as Polarization curves. Anodic and cathodic polarization curves allow determining the state of the corrosion reaction, i.e. both the corrosion potential (E_{corr}) and the corrosion current (i_{corr}) for a certain metal in that system. Various metals behave in different ways in an aqueous solution. Corrosion behavior of an anodic material can be studied using an Evans diagram, Figure 3-1. Diagrams which represent schematically the polarization curves of the anodic and cathodic reactions in relation to the corrosion potential and current are known as Evans Diagrams [12]. The different

possible translations and occurrences seen in the anodic behavior of different metals can be determined using this diagram. It is also vital for understanding and estimating qualitatively the effects of changes in corrosion potential and current on the polarization curves, which can also be understood from the Evan's diagram. It is a plot of the logarithm of the absolute value of current as a function of the potential.

From Figure 3-1, the different regions in the anodic behavior of a metal can be seen. As the curve proceeds from A-B and potential increases from E_{corr} to E_{pass}, it indicates that the metal is undergoing active dissolution. E_{pass} is the potential at which a thin layer of oxide film is formed and hence passivation occurs on the metal surface. It is due to this oxide layer formation that, on further increase in potential, the current either remains constant till a higher potential (from B to B') or drops to a much lower current value (from B to C). In in the case of a metallic oxide layer with poor electrical conductivity, the oxide layer is stable and thereby the current density value remains constant (from C to D). For a metal having an oxide layer with good conductivity, an evident increase in the current is seen at a certain high potential (at E) due to the evolution of oxygen during oxidation of water. If the oxide layer is composed of cations which can be oxidized to higher oxidation state forming soluble products an increase in current may occur at lower anodic potentials (at F) accompanied by the dissolution of

metal due to transpassivity. In many metals and alloys which exhibit passive behavior, due to presence of halide anions in the aqueous solution, the oxide layer becomes locally unstable at a certain critical potential. Due to the breakdown of the passive layer, a sudden exponential increase in the current (at G) leading to various forms of localized corrosion is seen. At the metal/solution interface if chemical micro or macro heterogeneity is developed in correspondence to the system morphology, it can be classified as pitting or crevice type of corrosion. While in the metal itself, if there exists a chemical micro heterogeneity, selective dissolution or intergranular attack can occur.

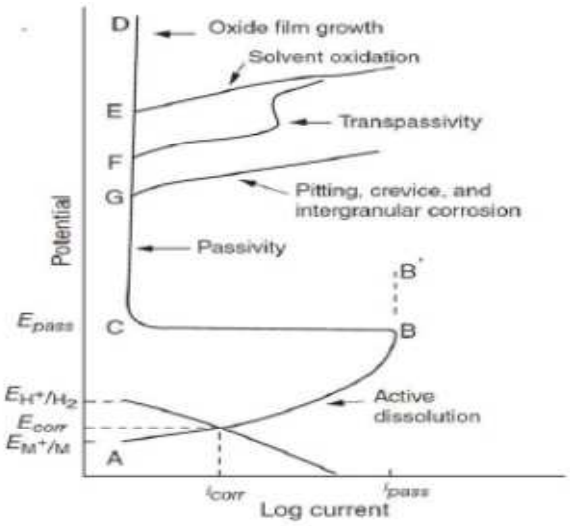

Figure 3-1: Variations of anodic behavior of passivating metals seen in aqueous solutions [13].

3.3 Types of Corrosion

Most metals tend to undergo corrosion when in contact with aqueous solutions (or moisture), salts, acids, oils and reactive materials. Uniform type of corrosion is seen in most cases when metals are subjected to these conditions. Metals that corrode uniformly are known to have an active nature in that particular solution. Some basic structural steels, like 1018 and 8620, are active-metals and exhibit uniform corrosion in most aqueous solutions. However, some metals exhibit active-passive behavior in aqueous solutions. For example, stainless steel like 304 and 416, nickel and titanium are resistant to corrosion. They form an oxide layer on the metal surface which acts as a passive layer and inhibits corrosion. Such metals that passivize may undergo a localized type of corrosion known as pitting corrosion. Pitting corrosion forms tiny pits or holes in the metal component and occurs due to the breakdown of its passive layer or presence of a defect or any dissimilarity in its passive layer. In some cases, the passive layer can be worn off due to erosion or abrasion by mechanical or other types of forces which can repeatedly wear off its passive layer and cause continuous loss of the meal component. Furthermore, there are many types of corrosion that can be caused due to different environments and forces involved. A classified form of most commonly seen types of corrosion based on material and driving force are given in Table 3.1.

Table 3-1: Table illustrating the types of corrosion based on the system and driving force [2]

Type of Corrosion	Material System	Driving Force	Control Point	Remark
Uniform/General Corrosion	All Metals in Atmospheric Environment	- Atmospheric -Temperature	- Painting - Hot Dip Galvanizing	- Corrosion Cost of this form about 50% of the total corrosion cost - Seldom lead to failure
Intergranular Corrosion	Al Alloys, Ni-Cr Austenitic Stainless Steel Acids Containing Oxidizing Agents (sulfuric, phosphoric), Hot Organic Acid. High Cl Content Seawater	-Third Phase Precipitate - Temperature	- Heat Treatment in Manufacturing - Welding during Fabrication	- Loss of Strength and Ductility - Severe attack can lead to failure
Galvanic Corrosion	Galvanic Coupling Materials e.g. Fe with Cu, Carbon steel with Stainless Steel	Different Metal in electrolytic solution	- Proper Design; - Rivetting/Joining Materials; - Insulating Coupling Materials	Moderate effect but can be detrimental for a longer period
Crevice Corrosion	Metal to Metal/Non Metal in Electrolyte Metal in two Electrolyte Aluminium and Stainless Steel in Seawater	- Small Gap in electrolyte (<3,18mm) - Stagnant Fluid	- Proper Design - Gasketting Materials -Proper Drainage Practice	Moderate effect but can be detrimental for a longer period
Pitting	Stainless Steel and Aluminium in cloride or bromide environment (water/soils)	- Surface Irregularities - Presence of Cl or Br Ion - Chemical Composition - Temperature	- Surface Quality Control - Proper Welding Practice -Proper Material Handling - PREN (Material Selection) - CPT (Critical Pitting Temperature)	Severe attack can lead to failure (second biggest corrosion failure)
Erosion Corrosion Tribo-Corrosion	Carbon Steel, Stainless Steel in flowing fluid containing abrasives	Synergy effect of passive film breakdown by abrasive and localized corrosion	Corrodent; turbulency Corrodent impingement in elbow and tees	Severe attack can lead to failure
Stress Corrosion Cracking (SCC)/ HE-SCC	Stainless Steel, Carbon Steel in High pH (pH >9,3) - 600 - 750 mV - Temperature Sensitive Near Netral pH (5,5 - 7,5) - Free Potential - Non-Temperature Sensitive	- Microstructure - Temperature Region - Existence of Residual Stress - Suitable pH - Presence of H_2S, Chloride ion -Residual Stress	- Microstructure Control during - H_2S Content & Temperature - Operation Temperature	-Biggest Cause of Corrosion Failure -SCC found in gas and liquid pipelines - In Canada since 1977: recorded 22 catastrophic failure (12 rupture, 10 leaks)
Biological Corrosion/ Microbial Induced Corrosion	All Metals in Environment with: - Sulfate Reducing Bacteria - Sulphur/Sulfate Oxidizing Bacteria - Fe/Mn Oxidizing Bacteria - Organic Acid Producing Bacteria	- Gravitational & Pellicular Water - pH 6 - 8 - Potential -42mV to 820mV - Temperature: 20 °C - 45 °C	Application of Organic Coating Cleaning Practice Use of Biocide	In US, $1.2 billion SPENT annually on biocidal chemicals to fight MIC.

3.4 Electrochemical Nature of Metals

Different metals exhibit different behavior when their electrochemical nature in various aqueous, neutral, acidic and basic solutions is considered. Neither is there any change observed in the cathodic polarization curves for reduction of hydrogen ions or oxygen molecules nor in the reversible potentials for these reduction reactions as well. But, there is a change in the exchange currents and Tafel slopes of the polarization curves may considerably differ. The corrosion potential of a metal may be affected by the formation of an oxide film, and the tendency to form such a film is related to the standard electrode potential for the electrochemical reaction. The standard corrosion potentials of metals in aggressive solutions (that include chlorides) at which an oxide layer can be formed, does not always mean that the oxide layer forms at those potentials and hence differs from the standard electrode potential for metal/metal ion reactions. The factors that control the oxide layer formation potentials are (a) oxide solubility; (b) kinetics involved; additional activation potential may be required for oxide formation at significant rate; (c) instability due to action by aggressive solution ions, e.g. chloride. Ti has the most noble corrosion potential despite its very negative thermodynamic standard potential for metal ion formation. It is because it actively passivates forming a very protective oxide film at even very negative potentials, and the oxide film has significant resistance to breakdown by

chloride ions (highly corrosion resistant film). In the case of chromium and aluminum, the potential has a considerable noble range due to the formation of oxide films, but these are partially broken down by chloride ions giving rise to localized corrosion. On the other metals, oxide films do not behave as protective films due to the action of chloride ions, or film instability. Thus, corrosion rate in aggressive solutions is then controlled mainly by the magnitude of the reversible potential for the metal/metal ion reaction in relation to the cathodic polarization curves for oxygen and water reduction (as illustrated in Figure 3-2) [12]. The figure illustrates the anodic polarization curves of copper, iron and zinc intersecting the cathodic reduction curve of oxygen, which causes a negative shift to the corrosion potentials and corrosion currents in the order, copper<iron<zinc.

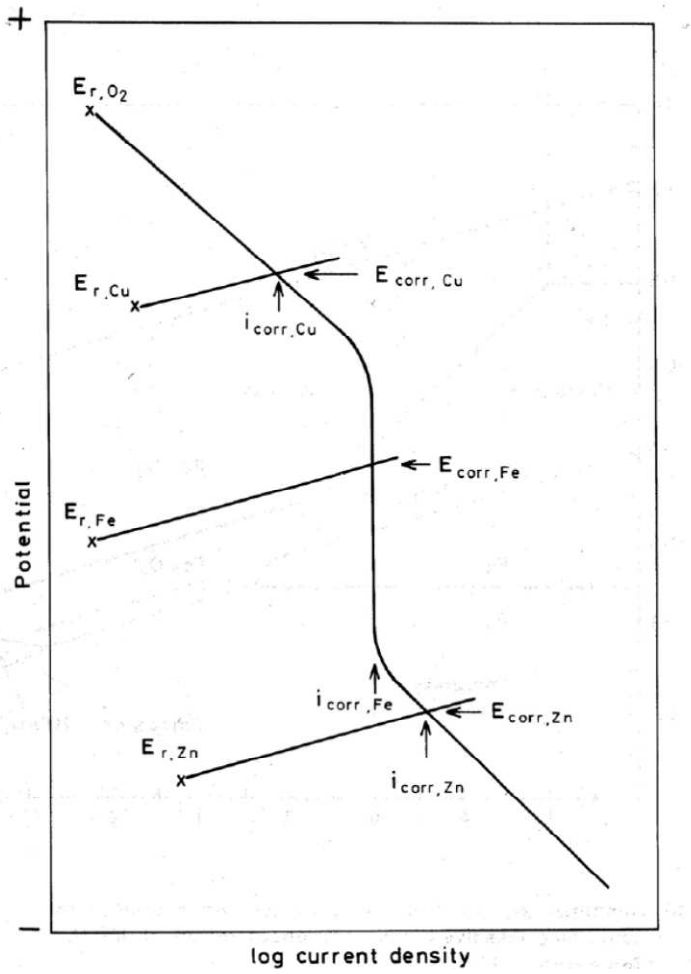

Figure 3-2: Metal/metal ion reversible potentials in relation to the cathodic polarization curve for oxygen reduction [12]

Understanding the basic thermodynamics involved is important to study the electrochemical behavior of metals. As discussed previously, formation of an oxide film on metal surfaces is a critical aspect of corrosion protection. Figure 3-3 illustrates schematically the anodic and cathodic polarization curves of a system

where passivation is possible, e.g. stainless steel in dilute acid solution. If the solution is de-aerated, the cathodic reaction will be reduction will be reduction of hydrogen ions with a cathodic polarization curve (UV) which intersects with the anodic polarization curve (ABCDE) at V, corresponding to corrosion in its active state, which determines the corrosion rate and corrosion potential.

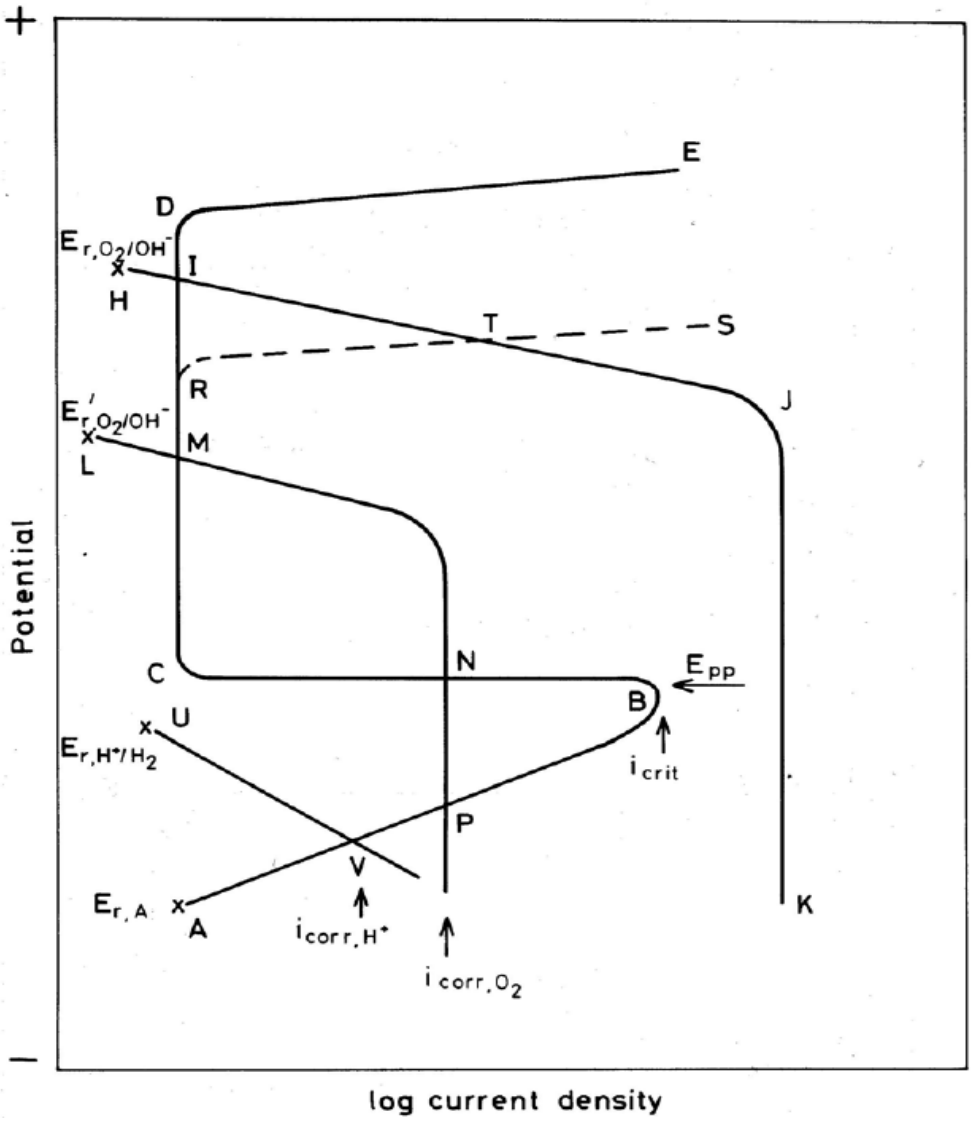

Figure 3-3: Schematic of polarization curves for corrosion, passivation and passive film breakdown for stainless steels in dilute acid solutions [12]

Corrosion behavior of Fe has been greatly studied by several researchers, due to its high importance, it being a main constituent of most metallic construction materials. Complex corrosion process of Fe has been analyzed by carrying out most research on its anodic behavior in sulphuric acid solutions. The potentiodynamic anodic polarization curves deduced of Fe in sulphuric acid solution can be divided in four sections [13, 14]. At low polarization in the active anodic section, i.e. the Tafel section, the overall metallic dissolution of Fe is charge transfer controlled [13-17]. The active dissolution phase is followed by a transition phase, characterized by adsorbed $Fe(OH)_{2,ads}$ on the electrode surface. A maximum-minimum behavior of the current density was noted for the transition phase and was related to the adsorbed fraction of $Fe(OH)_{2,ads}$ [14-18]. Later, Schweickert et al [18] reported a plateau of the current density instead of a maximum-minimum nature.

According to thermodynamics, an electrochemical reaction is reversible at its equilibrium potential, where no net reaction is observed. The thermodynamic prediction of metallic corrosion behavior was illustrated by Pourbaix [1] in the form of potential-pH diagrams. Figure 3-4 shows a simplified Pourbaix diagram of iron in aqueous solutions in which no complex ions are formed and the oxides or iron are the only stable solid phases. The Pourbaix diagram is calculated for concentrations of dissolved iron of 10^{-6} M and for at a temperature of 25°C. The

various stages of iron can be seen at the given pH and potential values, viz passivating, corrosion (ionic form) and immunity (stable metallic form).

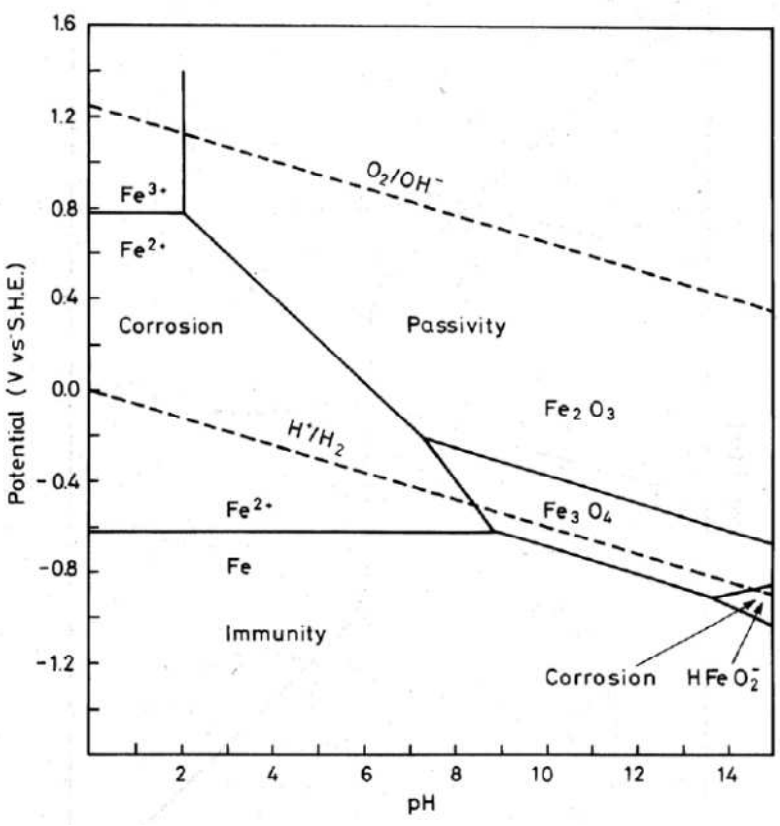

Figure 3-4: Simplified potential-pH diagram for iron in a solution containing dissolved iron at a concentration of 10^{-6} M at temperature 25°C [12].

3.3 Magnetic Field Effect on Corrosion Behavior

Magnetic field effects on electrochemical behavior of metallic materials have been recently studied with great interest by researchers [5,19-42]. According to literature, a magnetic field can influence metallic corrosion by acting on the

electrode kinetics [44-45], on the mass transport [46-51], on the formation of an interfacial oxide/hydroxide layer [52-55] or on the potential difference at the metal solution interface [56]. In magnetoelectrochemistry, i.e. in electrochemistry influenced by external magnetic field, different forces of magnetic origin are hence found and actively debated by many researchers. An overview of these forces under discussion can be found in [11]. Recently, the so-called 'concentration gradient force' or 'paramagnetic gradient force' [11] has attracted much attention, can be seen in [56-64]. According to documented arguments in favor of the existence of this force results from the unexpected low deposition rates of metal, e.g. Cobalt ions, in presence of a magnetic field [59].

Magnetohydrodynamic theory (MHD) is generally used to formulate the effect of magnetic fields on mass transport rates, which has been reviewed in Refs. [19-20]. Magnetic fields can affect electrochemical reactions, especially mass transport rates, i.e. limiting current density, for metallic materials in aqueous solutions [16-20]. The main effect of a magnetic field applied on an electrochemical system is the introduction of additional forces on the ions in the electrolyte [15] and also called as the "MHD effect". These effects of magnetic fields on the electrochemical process involving mass transport and Lorentz force generated due to the magnetic fields, have also been analyzed based on the MHD theory [16-20]. Figure 3-5 depicts the schematic of the overlapping and

perpendicular magnetic-electrical fields, giving rise to Lorentz Force in a direction mutually perpendicular to both the fields.

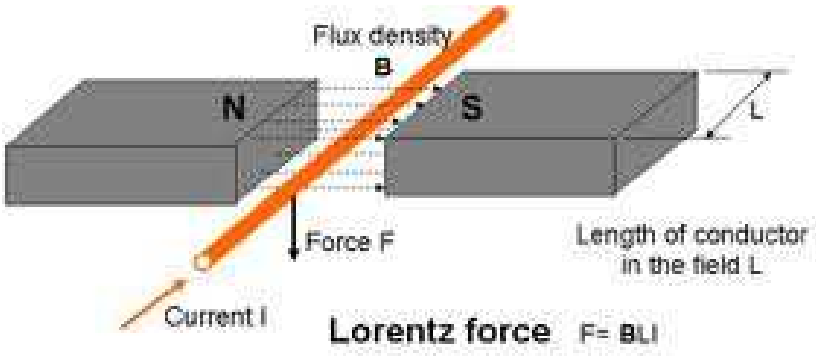

Figure 3-5: Schematically representation of induced Lorentz force in the presence of mutually perpendicular magnetic and electrical fields [2].

Compared to both the paramagnetic gradient force and Lorentz force, the former one is more widely accepted and established force in magneto electrochemistry. In the case when the magnetic field is normal to the working electrode (WE), i.e. the magnetic field lines are parallel to the electric field, then Lorentz forces are often assumed to be absent. Even if this can be accepted to be the real scenario in the direct vicinity of the WE, Lorentz forces can still originate at the areas anywhere else in the cell where both the electric and magnetic field are not strictly parallel. Thereby, the convention arising from the Lorentz forces in the aqueous solution, will influence the electrochemical reaction kinetics and mass transfer at the electrode since it is generally not always confined to its

origin. This scenario is even more seen in small cells which have to be used in the narrow gaps of electromagnets. Besides the finding that the magnetic field gradient force can dominate the electrode behavior, the impact of high magnetic flux densities and high gradients of the magnetic flux density on corrosion processes has barely been investigated. Furthermore, polarization experiments reveal integral information over the whole electrode surface, but for application a localization of the corrosion reaction is of very practical importance [65].

Unlike most researchers, Weier et al [66], in their study of magnetic field effects on electrochemical reactions, concentrated and observed convection arising in the solution and its direction. They tried to identify whether a possible paramagnetic gradient force or Lorentz force is responsible for the confinement of the paramagnetic ions at the electrode surface, in the presence of a magnetic field. In their research, to measure the flow fields, an easily applicable measurement technique named Particle Image Velocimetry (PIV) was used. Interferometry, was used previously by O'Brien and coworkers e.g. [56, 67], to measure concentration fields in the electrochemical cells under magnetic field influence. For a more practical and compatible system to PIV system, background oriented schlieren (BOS) [68] was used for concentration configurations in this research. The main objective of this research was to demonstrate the Lorentz force generated convection at milielectrodes via PIV while the corresponding concentration

variations were visualized by BOS and interferometry. On analyzing keenly the important reactions such as deposition, dissolution and the electrochemical behavior by switching back to open circuit potential, they did not find any influence of the paramagnetic gradient force, necessary to explain convection in the solution. By experimental observations, they concluded that the confinement of paramagnetic ions at circular electrodes is caused to a large extent by Lorentz force driven convection only.

3.3.1 Magnetic field effect on anodic behavior of ferromagnetic materials

In the case of iron, some fundamental studies on effects of magnetic field on its anodic polarization behavior in strongly acidic solutions [40, 69] and weekly alkaline solutions [42] and neutral solutions [70] have been carried out. In weekly acidic buffered solutions no investigations are reported yet. In the study by Tang et al [69] and few other researchers [40, 42], it was shown that the passivation potential shifts to a more noble value with an applied magnetic field, especially with the magnetic flux perpendicular to the electrical charge flow. The common explanation given to this phenomenon is the MHD effect driven by Lorentz forces.

However, iron gets magnetized under the influence of a magnetic field attributing to its ferromagnetic nature. The magnetized iron electrode leads to a strongly inhomogeneous stray field over the surface with a flux density which can

overcome the external one. Ragsdale et al [33] demonstrated that paramagnetic molecules are concentrated at the iron electrode surface due to the magnetic field gradient force. This increased concentration at the electrode surface can become important during the dissolution and passivation of a ferromagnetic electrode itself, especially when the effect of Lorentz force is minimal. Lu et al [71] reported an impact of an applied magnetic field on the surface structure after anodic dissolution of Fe. A characteristic patterning of the cross-sectional area of a Fe cylinder after anodic polarization in sulphuric acid with a magnetic field applied parallel to the investigated surface was observed and explained by Lorentz force driven convention. Quantitative information or study on the field driven localization of the corrosion, especially the impact of very high magnetic flux densities, is not yet been reported. Furthermore, magnetic field effects in different electrolytic concentrations were also studied.

Sueptitz et al [72] studied the electrochemical behavior of a ferromagnetic electrode in acidic solution under external influence of an applied magnetic field and depending on the orientation of its field lines. An iron wire was used in 0.5M sulphuric acid solution (pH 0.25) and 0.5M phthalate buffer (pH 5) under the influence of a 0.6T homogenous magnetic field.

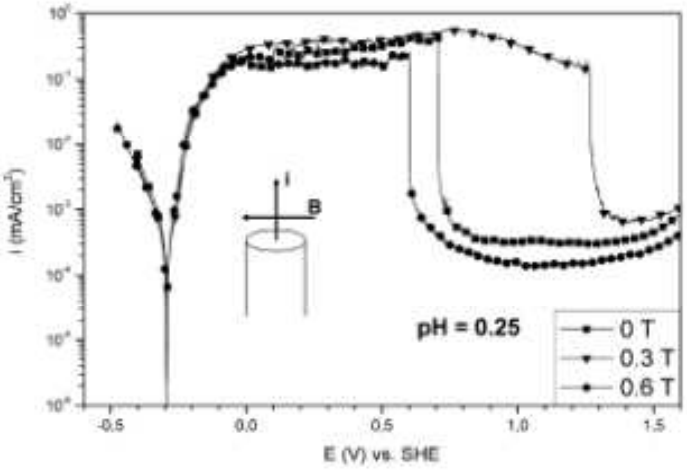

(a)

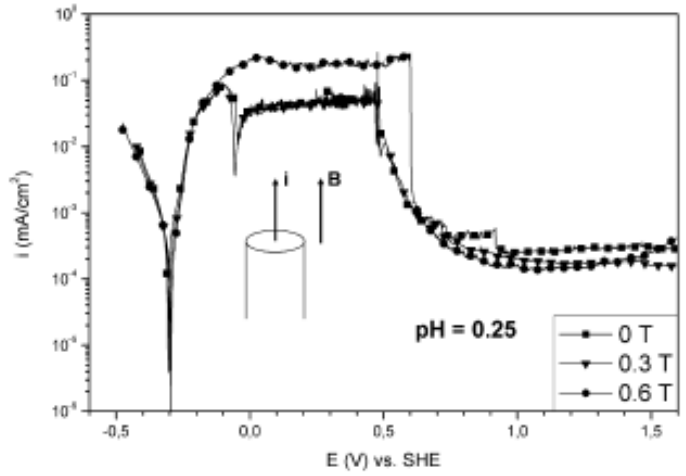

(b)

Figure 3-6: The potentiodynamic curves of iron in phthalate buffer (pH 5) without and with magnetic field applied (a) parallel and (b) perpendicular to the electrode surface (scan rate of 0.5mV/s) [72].

The potentiodynamic polarization curves recorded for the iron wire in sulphuric acid solution (pH 0.25) without and with magnetic field applied parallel to the electrode surface are shown in Figure 3-6 (a). While, when applied magnetic field is perpendicular to electrode surface in shown in Figure 3-6 (b). It was found that when the applied magnetic field is parallel to the electrode surface there is no much effect on the OCP. While there is considerable effect on the current density in the diffusion-controlled region, which increases from i_{max}=120 mA/cm^2 without applied magnetic field to i_{max}=540 mA/cm^2 at a flux density of 0.6T and the potential of the active-passive transition region is shifted to more noble values, i.e. 7000 mV at 0.3T and 1250 mV at 0.6T, respectively. These results were also reported by Lu et al [40]. The results were attributed to an additional convection of the electrolyte driven by the acting Lorentz force, which has its maximum in this field configuration [73].

Current-density curves obtained in sulphuric acid when, the magnetic field is applied perpendicular to the electrode configuration, are observed to show not much variation when compared to its counterpart. The maximum current density is reached at -100 mV with applied magnetic field and followed by constant current density which is about one tenth of the limiting current density reached without applied magnetic field. The passive current density is not significantly

affected but he active-passive transition appears to occur much earlier, i.e. at much more negative potential.

The anodic behavior of iron in phthalate buffer differed strongly from the behavior observed in the sulphuric acid solution as shown in Figure 3-7 (a) for parallel magnetic field configuration and (b) for perpendicular field configuration. The OCP adjusts at much more anodic values and the current density was observed to be one order of magnitude lower. Low dissolution rates are observed from which it is inferred that, a Lorentz-force driven convection shows no significant effect on the current density. By further increase of flux density the active-passive transition potential is shifted to less noble values and the passive current density is decreased, which cannot be explained by a MHD effect. While, in the case when magnetic field is applied in perpendicular direction the current density during active dissolution slightly increases, the active-passive transition potential shifts towards negative direction and the passive current density is lowered to about one tenth of its value at 0T. As observed in the case of magnetic field effect in sulphuric acid solution, the effect does not change on increasing the flux density from 0.3T to 0.6T.

It was firstly concluded that the Lorentz force only affects the dissolution and passivation behavior of an iron wire in acidic environment when the anodic reaction is diffusion-controlled in the active-region. When the magnetic field is

applied perpendicular to the wire cross section, a homogenous maximum flux density occurs at the rim of electrode surface. In this configuration, field gradient force dominates the Lorentz force effect which leads to decrease in the diffusion-limited current density and a negative shift of the active-passive transition potential. This is presumably due to a favored passive layer formation at the rim of the electrode, which expands towards the center with progressing passivation. Secondly, in phthalate buffer solution, the anodic dissolution rate is not diffusion-controlled and only affected by the field-gradient force.

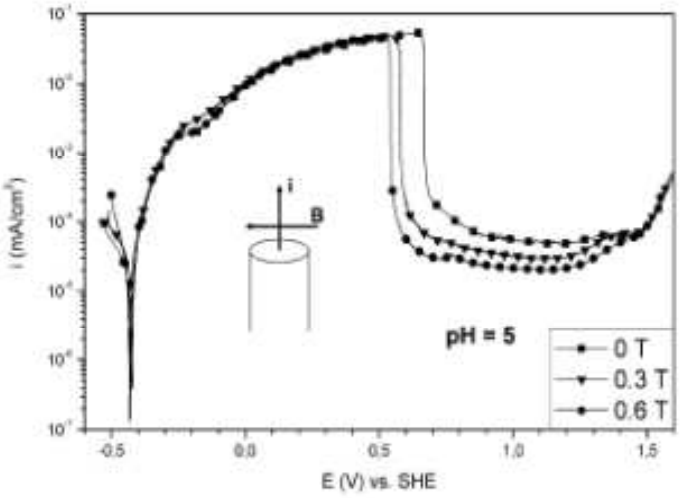

(a)

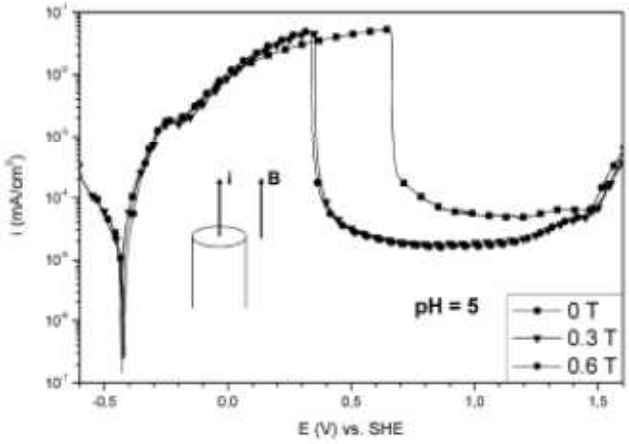

(b)

Figure 3-7: The potentiodynamic curves of iron in phthalate buffer (pH 5) without and with magnetic field applied (a) parallel and (b) perpendicular to the electrode surface (scan rate of 0.5mV/s) [72].

3.3.2 Magnetic Field effects on corrosion behavior of non-ferrous alloys

In comparison to the large number of available reports on the study of magnetic field effect on the mass transport behavior for metallic materials in aqueous solutions [5, 19-26], relatively few reports are available on the study related to effect of magnetic field on the electron-transfer process [27-33]. Kelly [55] has studied the effect of magnetic field on the electrochemical behavior of Ti in flowing sulfuric acid. The electrochemical system chosen for their study, titanium in 1N H_2SO_4, was studied extensively in the absence of magnetic field [29] and was one in which the interfacial reactions, the oxidation of titanium to form Ti (III) ions in solution and the hydrogen evolution reaction, are both under activation control. Changes of the open-circuit potential (OCP) difference between two Ti electrodes were found to increase with increasing applied magnetic flux density in the range of 0-2.0 T in their study. The potential difference was found to be directly proportional to the magnetic flux density and, consequently, in contrast to relatively small value observed in their work (Δ=0.25 V at B=2.0 Tesla), Δ would attain a value of 1.5 V at B= 12 Tesla, all other factors remaining constant.

Electrodeposited coatings of zinc-nickel alloys have attracted much attention in the revolutionary world, due to its high corrosion resistance and better mechanical characteristics than pure zinc or other zinc-alloys [74-82]. Several

authors have proved that Zn-Ni alloys have the best corrosion behavior in saline environment [83-84]. Corrosion behavior can be altered by many factors such as morphology, or crystallographic phase composition. Albalat et al found that the presence of particular additives in the electrolyte media improved the surface homogeneity, which leads to better corrosion resistance even for an alloy with low Ni content [85]. A way to obtain different composition phases and alloys is to superimpose a magnetic field during co-deposition process [86-99]. When an electrochemical co-deposition is undertaken under magnetic field, convection in the electrolytic solution is induced (called MHD effect as discussed earlier). Fahidy reported that surface roughness could be decreased by MHD effects on the surface three-dimensional deposit film structure [90]. Devos et al reported that a magnetic field could change the surface morphology and the preferred orientation of the nickel grain due to an increase of the diffusion flux of specific inhibiting species [92].

Electrochemical corrosion behavior in NaCl medium of zinc-nickel alloys electrodeposited under applied magnetic field was studied by Chouchane et al [100]. In their research, electrochemical electrodeposition of zinc-nickel alloy coatings from sulfate bath was been carried out under low and high applied magnetic field and its influence on alloy structural parameters was discussed. They concluded that, the magnetic field can significantly improve the corrosion

resistance of alloys with low alloy nickel content. When the horizontal magnetic field has a low amplitude (B<1 T), the induced deposit roughness modification has no important effect on the corrosion behavior of the electrodeposited zinc-nickel alloy whereas the induced phase composition modification improves the polarization resistance of alloys which contain about 5 at% of nickel. When high magnetic field amplitude was involved, the morphology was not largely modified but the hydrogen reduction current dramatically decreased which lead to a large shift of the corrosion potential. This phenomenon was evidence for magnetic effect on the surface reactivity of electrodeposited alloys.

It is quite evident that most of the previous research work reporting magnetic field effects on electrochemical nature of materials were not studied in sea water solution in spite of its significance in real world. In this research, a near sea water solution, i.e. 3.5% NaCl solution was used to address this issue and characterize the corrosion behavior of selected engineering materials in this environment.

Chapter 4

EXPERIMENTAL

4.1 Materials

4.1.1 Materials Selection

To study the corrosion behavior of most common type of materials, specific materials were selected to distinguish the difference in the behavior between ferrous, non-ferrous, passivating and non-passivating as well as magnetic and non-magnetic.

Ferrous Alloys

304 Austenitic Stainless Steel: It is a grade of SS that shows an active-passive nature during corrosion due to its high Cr content. This material was used since it demonstrates passivation and is a non-magnetic ferrous alloy. Its nominal elemental composition is given in Table 4-1.

416 Stainless Steel: It is a grade of SS that also shows an active-passive behavior with an amount of Cr around 13%. However, its passivation ability is lower than that of 304 SS that has a much higher Cr content. This material was used since it demonstrates passivation and is a ferro-magnetic material. Its nominal elemental composition is given in Table 4-1.

1018 Low-carbon Steel: It is a most common type of steel known for its strength. This material was used since it is an active and a Ferro-magnetic material. Its nominal elemental composition is given in Table 4-1.

Table 4-1**:** Nominal elemental composition of 304 SS, 416 SS and 1018 Low-carbon Steel

Elements	**304 SS**	**416 SS**	**1018**
Carbon, C	<= 0.080 %	<= 0.15 %	0.18 - 0.23 %
Chromium, Cr	18 - 20 %	13 %	0.40 - 0.60 %
Iron, Fe	66.345 - 74 %	84 %	96.895 - 98.02 %
Manganese, Mn	<= 2.0 %	<= 1.25 %	0.70 - 0.90 %
Nickel, Ni	8.0 - 10.5 %	_	0.40 - 0.70 %
Phosphorous, P	<= 0.045 %	<= 0.060 %	<= 0.035 %
Silicon, Si	<= 1.0 %	<= 1.0 %	0.15 - 0.35 %
Sulfur, S	<= 0.030 %	>= 0.15 %	<= 0.040 %

Non-ferrous

Ti-6Al-4V alloy: This non-ferrous alloy was chosen since it actively passivates and is non-magnetic in terms of corrosion.

Pure Zn: Pure Zn was selected as it is non-ferrous, non-magnetic and is an active material.

4.1.1.1 Sample Preparation

Each sample was initially sectioned from 1 cm diameter rods to a length of about 1.6 cm. The sectioned samples were mounted in epoxy and threaded through the bottom edge, to be able to be suspended within the electrolyte as a WE. Prior to testing, the mounted samples were polished using a combined wet and rough grinder. Then, they were fine polished using emery papers of grids 320, 400, 600, 840 and lastly 1000 grid. A mirror-like surface finish (as shown in the Figure 4-1) was obtained using 1micron diamond paste on a cloth rotating grinder as the final step.

Figure 4-1 Sample as after preparation (with mirror finish)

4.1.2 Permanent Magnet

An NdFeB N50 permanent magnet was used for generating the magnetic field that was applied to the samples. The maximum magnetic strength of the magnet was 0.7 T, which was measured using a magnetometer.

4.1.3 Electrolyte

To simulate the salinity of sea water, 3.5% NaCl (sodium chloride) solution was used as the electrolyte for corrosion testing. The electrolyte was prepared by adding 35 g of sodium chloride salt crystals in 1000 ml of distilled water and stirred to produce a clear solution of pH = 6.8.

4.2 Electrochemical Testing

Electrochemical experiments were carried out to analyze the corrosion behavior and corrosion kinetics involved for all samples in 3.5% sodium chloride solution, both with and without the influence of a magnetic field. Initial baseline experiments were carried out with no magnetic field and then, followed by a set of similar experiments under the influence of a magnetic field. Both results and data were used to deduce and understand the magnetic field effect on the corrosion behavior of the selected materials.

4.2.1 Electrochemical Cell for baseline experiments

All electrochemical baseline experiments (without magnetic field) in this research were carried out in a K0047 Corrosion cell from Princeton Applied

Research, shown in Figure 4-2. As can be seen in the figure, the cell accommodates openings for the WE, reference electrode (RE), two counter electrodes (CE) and gas purge tube. It is a standard cell used to test and analyze the electrochemical reactions of metal specimens in aqueous solutions. The design of this cell is well-known and is used in many ASTM standards.

The cell can very well accommodate testing of a variety of metal specimens in most aqueous environments. It can be used in extreme conditions like, in highly aggressive environments (except HF), other than in ambient, in elevated temperatures as well and for long duration testing.

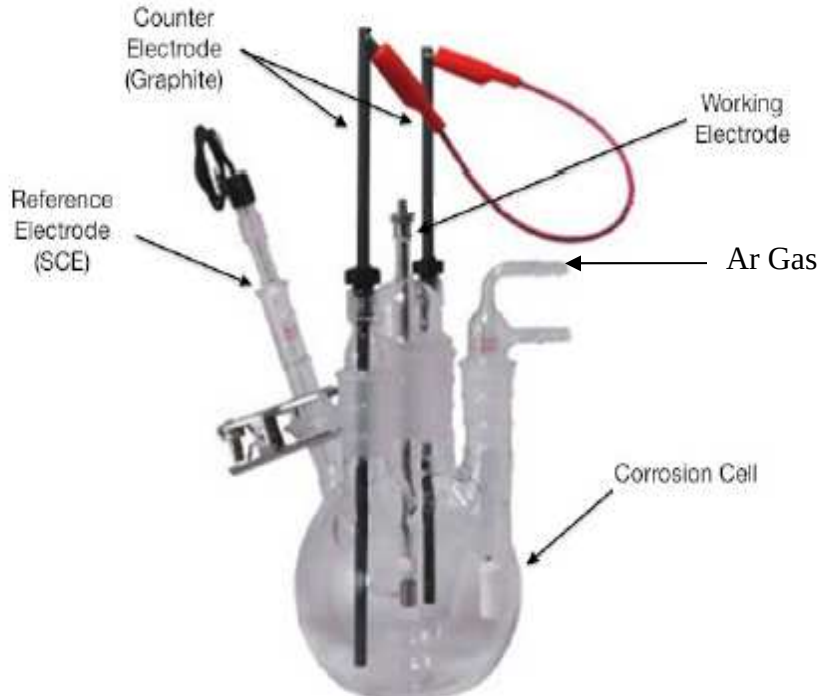

Figure 4-2: K0047 Corrosion cell from Princeton Applied Research

4.2.2 Electrochemical Cell for Magnetic field influenced experiments

Figure 4-3 shows the electrochemical cell that was designed with a similar configuration as the one used for the baseline experiments. The NdFeB N50 permanent magnet was placed externally adjacent to the working electrode, and such that the magnetic field was perpendicular to the sample surface.

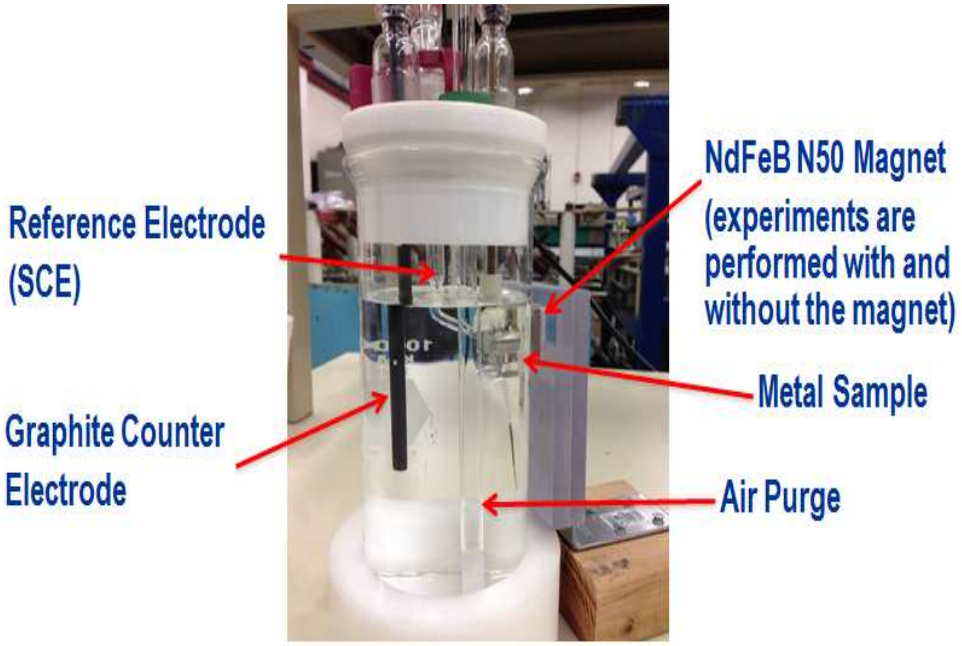

Figure 4-3: Electrochemical Cell with a NdFeN50 permanent magnet in the holder, attached alongside the cell

4.2.3 Electrochemical Testing

All electrochemical testing was performed using the above mentioned electrochemical cell. All samples were cleaned by rinsing with methanol prior to testing. Two graphite rods were used as CE and a saturated calomel electrode (SCE) as the RE. A double-salt-bridge was used between the electrochemical cell and the SCE reference electrode in order to prevent the contamination of chlorides

from the reference electrode [102]. A magnetic stirrer was used for agitation and to maintain uniform concentration in the electrolyte. The electrochemical cell was connected to an EG&G Princeton Applied Research Potentiostat/Galvanostat model 273A interface for all electrochemical experiments. This setup is linked to a Dell personal computer loaded with the 352 SoftCor III corrosion software used for electrochemical experiment's data acquisition and analysis. Figure 4-4 shows the electrochemical experimental laboratory set up present in the Surface and Nano-Engineering Laboratory (SaNEL).

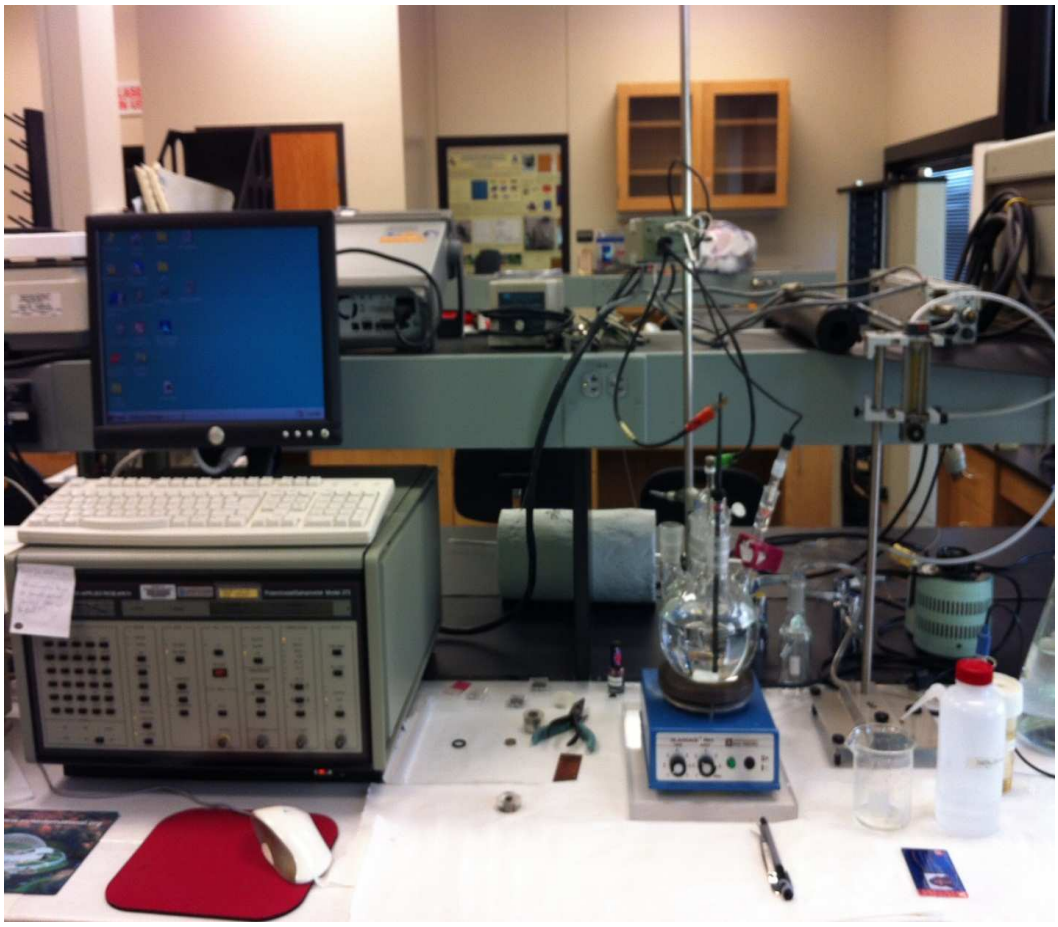

Figure 4-4: Electrochemical Testing experimental set-up available at SaNEL

4.2.3.1 Corrosion Potential vs Time Measurements

The open circuit potential (OCP), also referred to as the equilibrium potential, the rest potential, or the corrosion potential) is the potential at which there is no net current in the circuit. Hence, the experiments that are based on the measurement of the OCP are *potentiometric* experiments. A stable E_{OCP} was measured until the potential at the electrode surface was stable over time. All

electrochemical corrosion potential vs time experiments were carried out in aerated solutions (open to lab environment) until equilibrium was attained. Initially, a set of baseline experiments were carried out for all the samples without any magnetic field, followed by, a set of experiments for all samples with the external magnetic field applied.

4.2.3.2 Potentiodynamic Polarization Testing

To understand and analyze the corrosion behavior and kinetics of the chosen materials, potentiodynamic polarization tests were carried out in 3.5% NaCl aqueous solution. The tests were allowed to run by adjusting the initial potential to 200 mV below the OCP and carried on up to 600 mV above the OCP at a scan rate of 1 mVs^{-1}. All anodic polarization tests were carried out in aerated environment. Both baseline experiments and experiments influenced by external magnetic field were carried out with similar parameters and post data acquisition, Tafel exploration method was used to calculate corrosion rates.

4.3 Characterization

4.3.1 X-Ray Diffraction

X-ray diffraction (XRD) was used to determine the phases present in 304 SS sample only. The XRD pattern was obtained from a Siemens Krystaloflex 810 D500 machine. It was carried out by the low glancing angle method. The diffraction pattern was obtained by positioning the detector for 2□ values from

20° to 50° and the Cu Kα X-ray source (λ= 1.542Å) was at 10° (as shown in Figure 4-5).

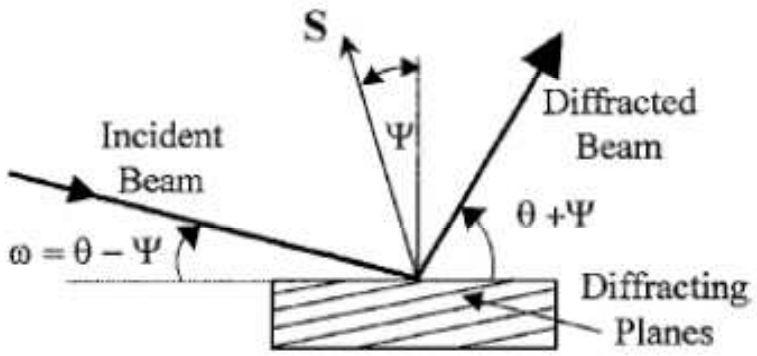

Figure 4-5: X-Ray Diffraction method to measure the intensity diffracted from the hkl planes at an angle Ψ to the surface of the specimen [103]

4.3.2 Scanning Electron Microscopy (SEM) and Energy dispersive Electron Spectroscopy (EDS)

All sample surface were characterized by Hitachi S-3000N Variable pressure SEM in conjunction with EDS. A working distance of 15 mm with high vacuum setting and electron voltage of 20-25 keV was used to obtain images before and after performing electrochemical testing. SEM micrographs were used to study and analyze the surface morphology and compare both micrographs of baseline samples and the ones of magnetic-filed influenced samples. In order to have a more clear understanding of the magnetic field effect at different regions

of the sample surface, scanning electron micrographs were captured at various magnifications and locations (edges and center).

Chapter 5

RESULTS AND DISCUSSION

5.1 X-Ray Diffraction analysis

The degree of magnetic response or magnetic permeability is derived from the microstructure of the steel. Figure 4-1 represents the XRD pattern obtained from 304 SS. It clearly shows two sharp peaks at 2□ values of 38.2 ° and 44.4° which represent the (111) and (200) planes of fcc austenitic steel respectively. From literature and according to Cheary et al [103], a characteristic peak at 45.5° represents the (110) plane of martensitic phase, which is not seen in Figure 4-1. According to a review published by the British Stainless Steel Association [104], the Austenitic structures are totally non-magnetic and so a 100% austenitic stainless steel would have a permeability of 1. Practically, this is not achievable. There is always a small amount of ferrite and/or martensite even in the austenitic steel and so permeability values are always above 1. Typical values for standard austenitic stainless steels can be in the order of 1.05 – 1.1 which is still very low to exhibit ferromagnetism.

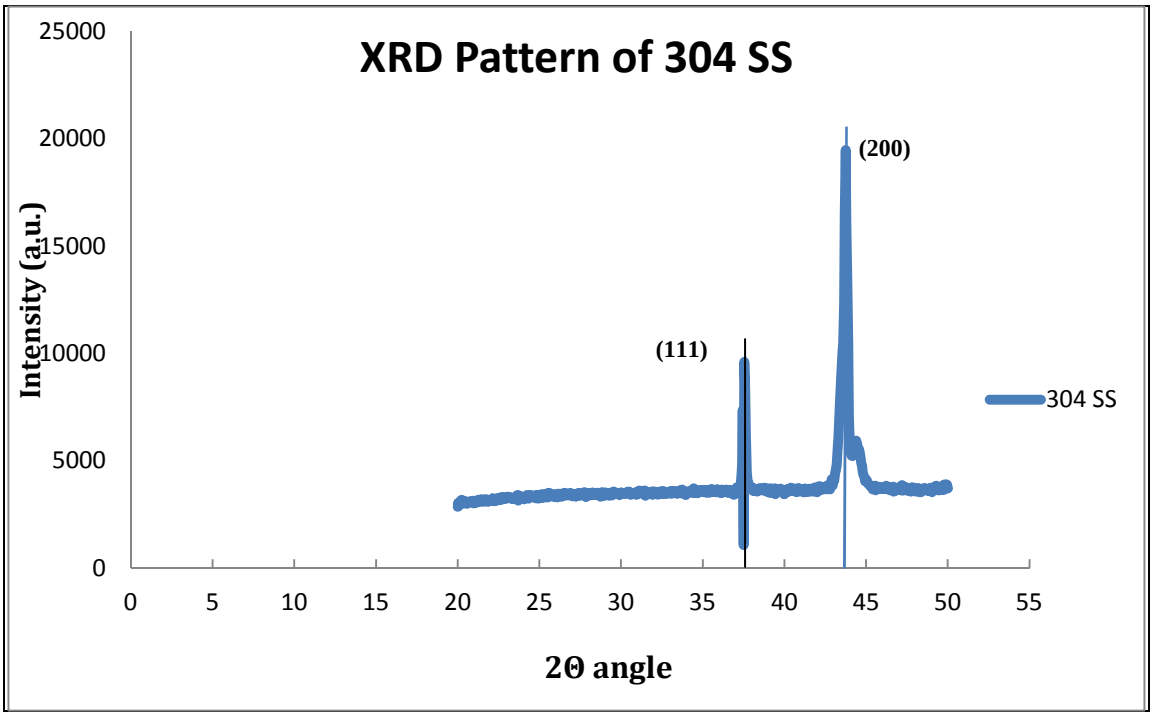

Figure 5-1: X-Ray Diffraction pattern of 304 stainless steel

5.2 Electrochemical Testing

Introduction

When an electrochemical reaction occurs at the metal-electrolyte interface, i.e. corrosion on the metal surface, it causes a shift in the potential of the system from the equilibrium half-cell potential. This is called polarization. During this phenomenon of loss of electrons from the metal, to transform into its ionic state, the deficiency of electrons causes a positive shift in the potential and this is called activation polarization. Current density measurement is also calibrated during

polarization tests because the corrosion rate directly depends on the amount of current per unit area.

As mentioned in the previous chapter of this research, potentiodynamic polarization tests and potential vs time measurements were carried out on ferrous alloys (i.e 304 SS, 416 SS and 1018 steel) and non-ferrous alloys (Ti6Al4V and pure Zn) both, with and without the influence of an external magnetic field under aerated conditions. Potential vs time measurements were carried out over variation with time. The final stable potential is also known as the corrosion potential (E_{corr}). At E_{corr} the system is said to have reached equilibrium or steady state at which all corrosion reactions are said to occur.

Anodic reaction involved in the electrochemical tests:

$M \rightarrow M^{n+} + ne^-$

where M is Fe for ferrous alloy tests which oxidizes to Fe^{2+} and M is Ti (oxidizes to Ti^{4+}) , Zn (oxidizes to Zn^{2+}) for titanium and zinc respectively.

Cathodic reactions involved in the tests:

$O_2 + 2H_2O + 4e^- \rightarrow 4OH^-$ (neutral aerated electrolyte) (7)

The standard reduction potential is +0.628 V vs. SCE

All corrosion experiments were carried out in aerated conditions and hence the possible cathodic reduction reaction is oxygen reduction. However, the reaction for hydrogen reduction reaction in deaerated solution is,

$2H_2O + 2e^- \rightarrow H_2 + 2OH^-$ (8)

The standard reduction potential is -0.632 V vs SCE.

5.2.1 Corrosion Behavior of Ferrous Alloys

5.2.1.1 304 Stainless Steel

The results obtained from the potential vs time measurements for 304 SS in 3.5% NaCl solution can be seen in Figure 5-2 (a). It illustrates the measurements obtained without and with the presence of an external magnetic field. The potential increases initially from -202 mV and -284 mV to a stable potential of -128 mV and -133 mV with time, when measured with and without magnetic field, respectively. On comparing the results of potential vs time measurements obtained with and without the presence of a magnetic field, as illustrated in the plot, it can be inferred that, there is no effect of magnetic field on OCP of 304 SS in 3.5% sodium chloride solution.

Figure 5-2 (b) illustrates the potentiodynamic polarization results of 304 SS in 3.5% NaCl solution in aerated conditions both, with and without the influence of an external magnetic field. The corrosion rate and corrosion potential for experiments conducted in both conditions are tabulated further in Table 5-1.

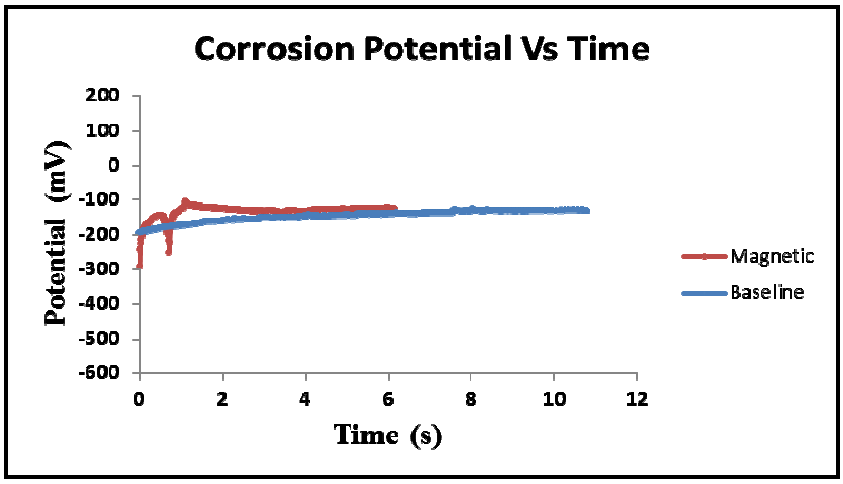

(a)

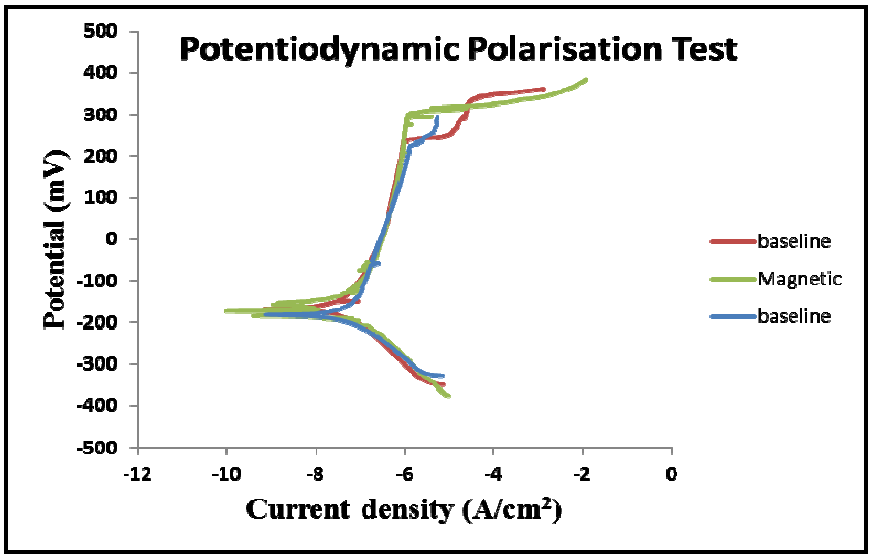

(b)

Figure 5-2: Comparison of results of (a) Corrosion potential Vs time measurement and (b) Potentiodynamic polarization curves of 304 SS in 3.5% NaCl, both without and with an external magnetic field.

Table 5-1: Potentiodynamic polarization curves report of 304 SS in 3.5% NaCl solution without and with an external magnetic field

Type	**Test 1**	**Test 2**	**Test 3**
Magnetic field strength, B (T)	0 T	0 T	0.7 T
Corrosion Potential (mV)	-196	-195	-192
Corrosion Rate ($\mu A.cm^{-2}$)	0.015	0.019	0.063

From the anodic polarization curves of 304 SS in 3.5% NaCl solution, a typical active-passive behavior can be seen. At the corrosion potential of -195 mV, it transforms from cathodic to anodic behavior. Further up till a small potential range above the corrosion potential, initial active dissolution is seen. From a potential of -100 mV the current density, of about 10^{-7} $A.cm^{-2}$, remains almost constant indicating passive region of 304 SS. The passive region ranges from a potential of -100 mV to 240 mV which is due to its highly stable oxide layer. After a significant long range of passive region, at a potential of about 245 mV a drastic increase in the current density is seen indicating the breakdown of the oxide layer (breakdown potential, E_B). The oxide layer breaks down at a potential of about -250 mV which is due to the action of chloride ions, giving rise

to pitting corrosion and formation of pits on the metal surface. Hence, it can also be called as the pitting or breakdown potential.

From the results of potentiodynamic polarization curves of 304 SS in 3.5% NaCl solution obtained with the impact of the external magnetic field, there is no significant change in the corrosion potential or corrosion rate when compared to the results obtained without an external magnetic field. However, two effects may be noted. First, the corrosion rate even though low for both conditions is higher under the influence of the magnetic field. It should be noted however, that 'corrosion rate' in this case describes the anodic current required for oxide formation rather than dissolution of some kind. Second, the results show that the E_B is somewhat higher (by about 50 mV) under the influence of the magnetic field. Both of the above observations are consistent with the effect of the magnetic field attracting oxygen at a higher pace thus, promoting and enhancing passivation.

The presence of the near hundred percent austenitic phase in 304 SS, as obtained from the XRD results, clearly explains the limited effect of the magnetic field on its corrosion behavior. Austenitic phase (i.e. gamma iron) is known to have very low relative permeability (~ 1.005) and that is why is called non-magnetic. Also, due to high Ni, Cr content, which not only act as austenitic

stabilizers, it even causes the electrode to readily passivate and thereby showing no impact of the magnetic field on the corrosion potential and corrosion kinetics.

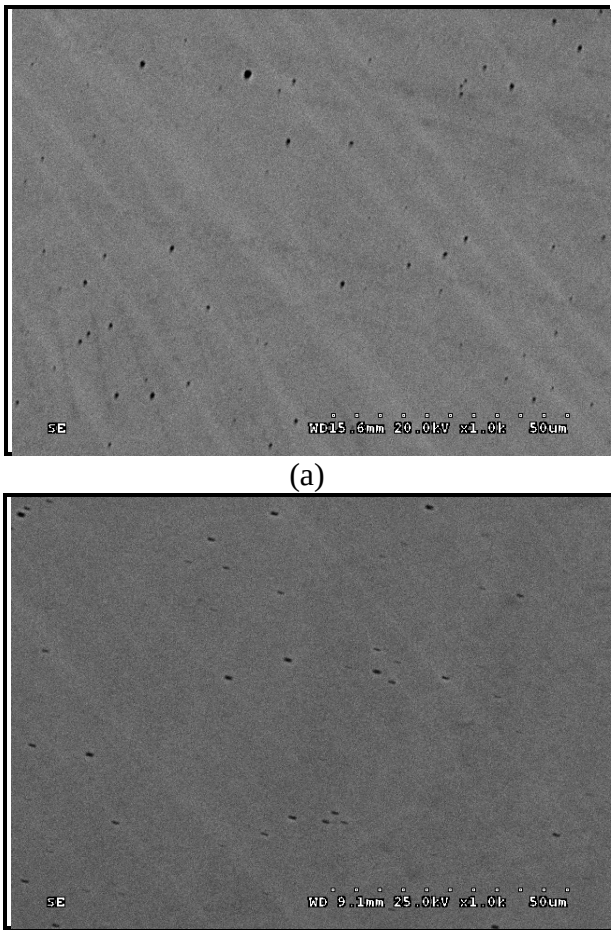

(a)

(b)

Figure 5-3: SEM micrographs of the edge and centre of 304 SS in 3.5% NaCl solution (a) without and (b) with impact of external magnetic field

Figure 5-3 (a) and (b) illustrates the SEM images of 304 SS in 3.5% NaCl solution taken after the OCP measurement tests, with and without an external magnetic field, respectively. It can be observed that the pit density and pit diameter are similar in both cases. The pits are observed to be homogenously spread on the metal surface and have a very small diameter (~0.4 µm). In support to the results of the electrochemical analysis, on comparing the SEM micrographs, it confirms that there is no significant effect of the magnetic field on 304 SS.

5.2.1.2 416 Stainless Steel

The results obtained for the OCP measurement and potentiodynamic polarization tests, with and without magnetic field influence are represented in Figures 5-4 (a) and (b), respectively. From the corrosion potential versus time response, it can be seen that the initial potential of -200mV decreases and stabilizes to -308 mV in the case without the magnetic field influence. Similarly, when there is an external magnetic field applied, the OCP decreases from a potential of -301 mV and stabilizes eventually at a potential of -410 mV. The magnetic field causes a negative shift of the OCP for 416 SS by about 100 mV. For a wide range below ca. 0.6 V corrosion of stainless steel is determined by the reaction.

$$Fe^{3+} + e^{-} \rightarrow Fe^{2+} \quad (9)$$

The anodic polarization curves of 416 SS in 3.5% NaCl solution is also observed to represent a typical active-passive behavior. However, its passive current density is not stable and much higher than that of 304 SS (a couple of orders higher). 416 SS is not exhibiting a fully passive behavior as shown by its anodic polarization curve. Due to the negative over-potential, the cathodic behavior is obtained and then at the corrosion potential, it changes and records its anodic behavior. It can be seen that, further up till a small potential range above the corrosion potential, active dissolution is seen.

From a potential of -200 mV the current density, of about 10^{-5}, not completely constant but shows a gradual increase, indicating passive region of 416 SS. The passive region ranges from a potential of -200 mV to 50 mV which is due to its considerably stable oxide layer. After the range of passive region, at a potential of about 70 mV a drastic increase in the current density is seen indicating the breakdown of the oxide layer. The oxide layer breaks down at a potential of about 70 mV which is due to the action of chloride ions, giving rise to pitting corrosion and formation of pits on the metal surface (E_B).

From the potentiodynamic polarization curves it can be seen that the corrosion potential has a negative shift from -303 mV to -408 mV due to applied magnetic field (0.7 T) in a perpendicular direction to the 416S S electrode surface in 3.5% NaCl solution. The current density also increases significantly from $10^{-7.4}$

$A.cm^{-2}$ to $10^{-5.5}$ $A.cm^{-2}$ due to the effect of the magnetic field. The negative shift in the corrosion potential and increase in current density integrally can be attributed to the impact of the magnetic field on the corrosion kinetics.

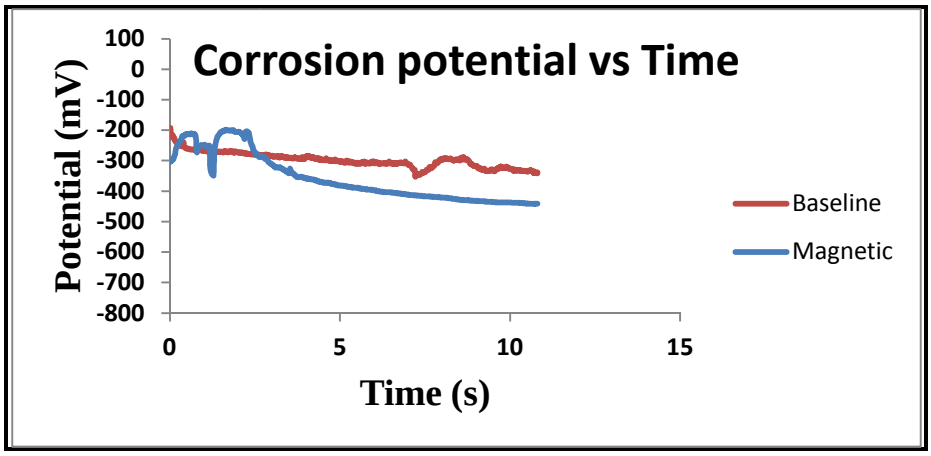

(a)

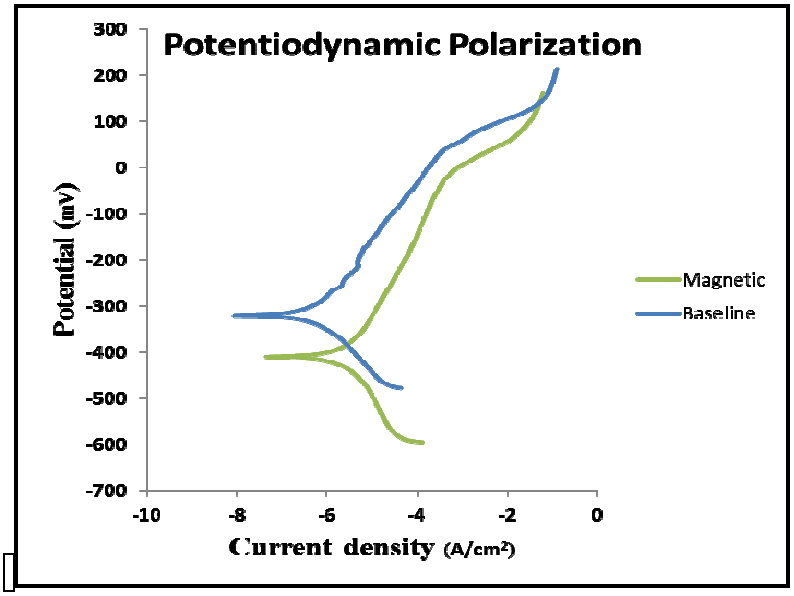

(b)

Figure 5-4: Comparison of results of (a) Corrosion potential Vs time measurement and (b) Potentiodynamic polarization curves of 416 SS in 3.5% NaCl, both without and with an external magnetic field

Table 5-2: Potentiodynamic polarization curves report of 416 SS in 3.5% NaCl solution with and without an external magnetic field

TYPE	**Test 1**	**Test 2**
Magnetic field strength, B (T)	0T	0.7T
Corrosion Potential (mV)	-308	-410
Corrosion rate ($\mu A.cm^{-2}$)	0.316	1.99

In Figure 5-5 (a) and (b) the SEM micrographs of both samples studied with and without the magnetic field influence respectively are illustrated. The difference in pit density and pit diameter at the centre and edges when compared to the baseline experiment's SEM micrographs can be observed. Due to the maximum flux density at the rim of the electrode a significant increase in the pit density, with smaller diameter are observed as compared to the homogenously distributed pits observed on the electrode surface of the experiments without a magnetic field. The different pitting pattern at the rim and center of the electrode surface due to the Lorentz force influenced convection was also confirmed by Linhardt et al [101]. Due to the higher velocity flow at the rim it promotes the repassivation tendency and thus causing a decrease in the current and associated

IR-drop. The smaller IR-drop causes an increase in the potential which triggers initiation of new pits and hence raising the current again. The interrelated mechanism involved at the electrode/surface interface reactions allows for a certain limited growth rate for pits and the altered potential and current density causes the high pit density with smaller diameter.

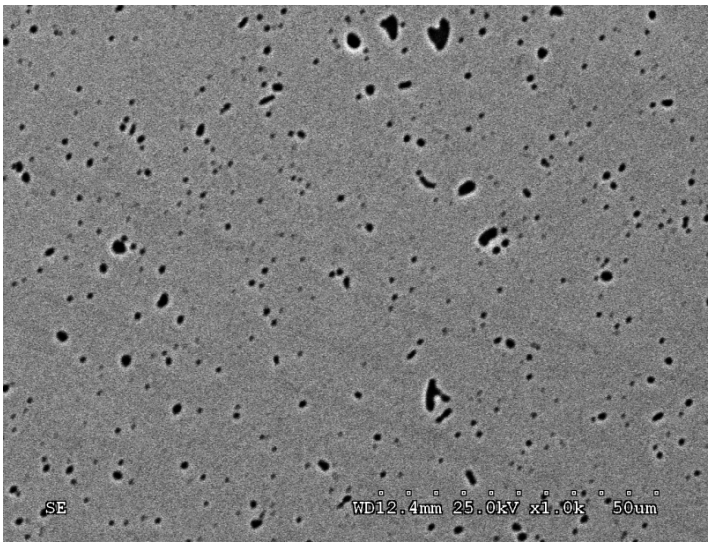

(a)

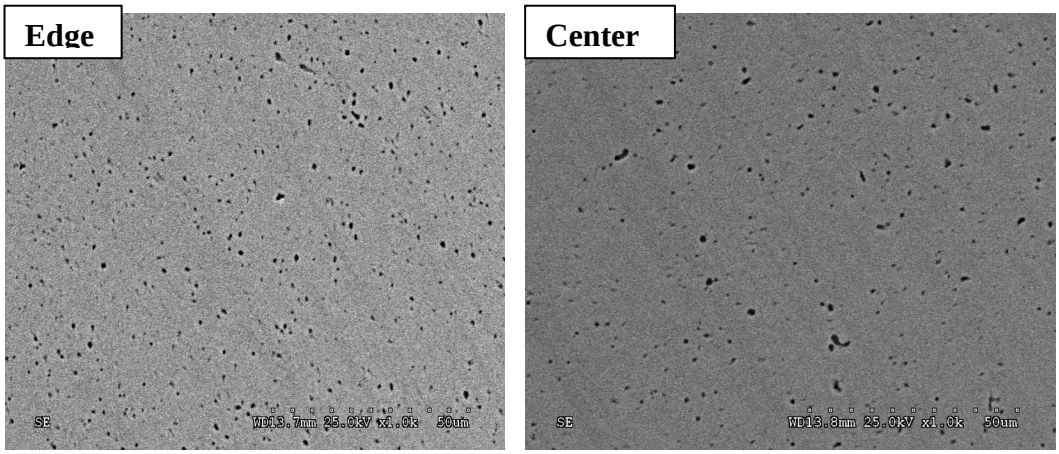

(b)

Figure 5-5: SEM micrographs of the edge and centre of 416 SS in 3.5% NaCl solution (a) without and (b) with impact of external magnetic field (both at edge and center)

5.2.1.3 1018 Carbon steel

The results obtained for the corrosion potential versus time measurements and potentiodynamic polarization tests, with and without a magnetic field influence are represented in the Figure 5-6 (a) and (b), respectively. It can be observed that the corrosion potential which initially is -548 mV decreases and stabilizes at equilibrium corrosion potential of -636 mV for baseline test. As seen in the case of magnetic test, due to the impact of the magnetic field, the initial potential of -560 mV, decreases and stabilizes at a potential of -710 mV. It causes a negative shift in the stable OCP of 1018 steel by about 110 mV. Similar observations were made for 416 SS in 3.5% NaCl solution due to the magnetic field.

Comparing the potentiodynamic polarization curves with and without the influence of a magnetic field, a significant impact is observed of the magnetic field on the corrosion kinetics. The corrosion potential shifts from -400 mV to -608 mV when an external magnetic field was applied perpendicular to the electrode surface of 1018 steel in 3.5% NaCl solution. The current density shows a considerable increase which means, a higher corrosion rate due to the magnetic field impact which is illustrated from the calibrated values seen in Table 5-3. It can also be confirmed by the higher Tafel slope as illustrated in the anodic polarization curves. As mentioned in the previous research, oxygen being

paramagnetic in nature is attracted towards the electrode surface and hence causes higher activity at the surface. The magnetic field induced Lorentz force promotes the mass-transport controlled reduction reaction also observed in research Lu et al [102]. The magnetic field has also found to effect the electron-transfer controlled Fe dissolution. The stray field on the electrode surface attracts paramagnetic oxygen which thereby increases the rate of electrochemical reactions.

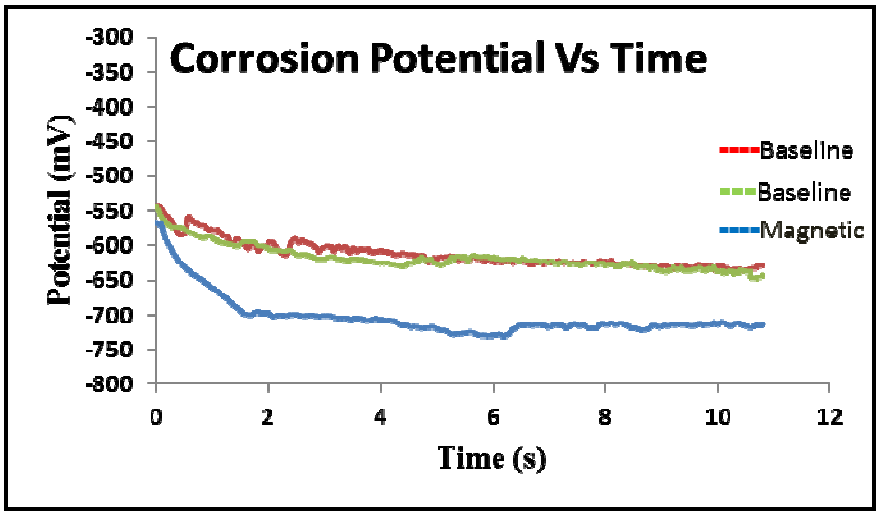

(a)

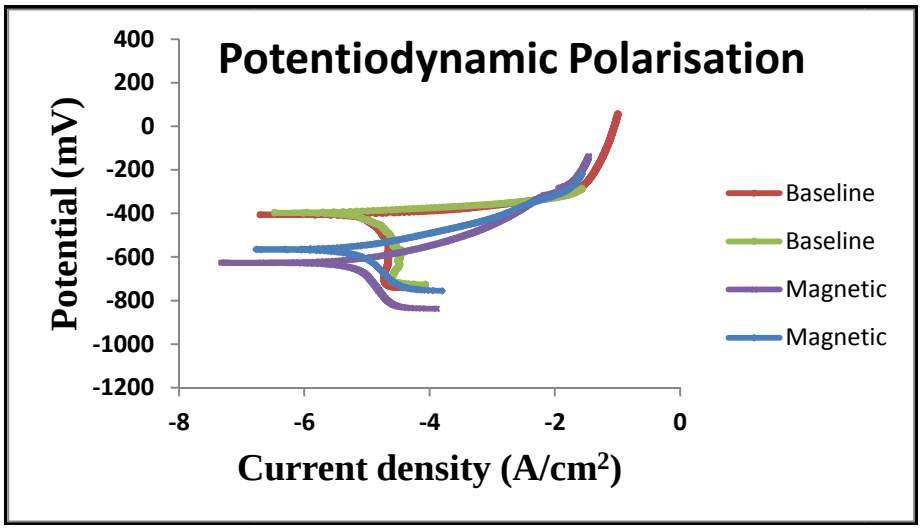

(b)

Figure 5-6: Comparison of results of (a) Corrosion potential Vs time measurement and (b) Potentiodynamic polarization curves of 1018 steel in 3.5% NaCl, both without and with an external magnetic field

Table 5-3: Potentiodynamic polarization curves report of 1018 steel in 3.5% NaCl solution with and without an external magnetic field

TYPE	Test 1	Test 2	Test 3	Test 4
Magnetic field strength, B (T)	0T	0T	0.7T	0.7T
Corrosion Potential (mV)	-400	-401	-596	-608
Corrosion rate ($\mu A.cm^{-2}$)	8.31	7.94	3.71	3.16

5.2.1.4 Zinc

The corrosion potential vs time and potentiodynamic polarization test results obtained for Zn in 3.5% NaCl, with and without the impact of an external magnetic field (baseline) are shown in Figures 5-7 (a) and (b), respectively. From Figure 5-7 (a) it can be see that there is no effect of the magnetic field on the OCP. The equilibrium potential is reached at -1003 mV and remains similar at -1008 mV when observed in 3.5% NaCl solution under the impact of the magnetic field. Also, from the Figure 5-7 (b), which compares the potentiodynamic polarization curves, in both conditions, the anodic behavior of Zn is seen. From the Tafel extrapolation, the corrosion rate and corrosion potential was determined and shown in Table 5-4. The values obtained from the Tafel slope extrapolation

confirms the very active dissolution of Zn observed in 3.5% NaCl solution with and without impact of a magnetic field.

Zn being an active material whose oxide layer deteriorates and causes further dissolution of the bulk in the chloride solution. It can be confirmed from the highly negative corrosion potential which is -1008 mV in 3.5% NaCl solution. No effect of the external magnetic field of 0.7 T is observed on Zn as it is a non-magnetic material. Also, Zn^{+2} ions are diamagnetic in nature due to their paired electron configuration. Zinc has zero unpaired electrons in its ionic state and hence is diamagnetic in nature. The driving force for active dissolution of the metal is larger than any other magnetic field driven forces in the electrolyte and therefore no major effect is seen.

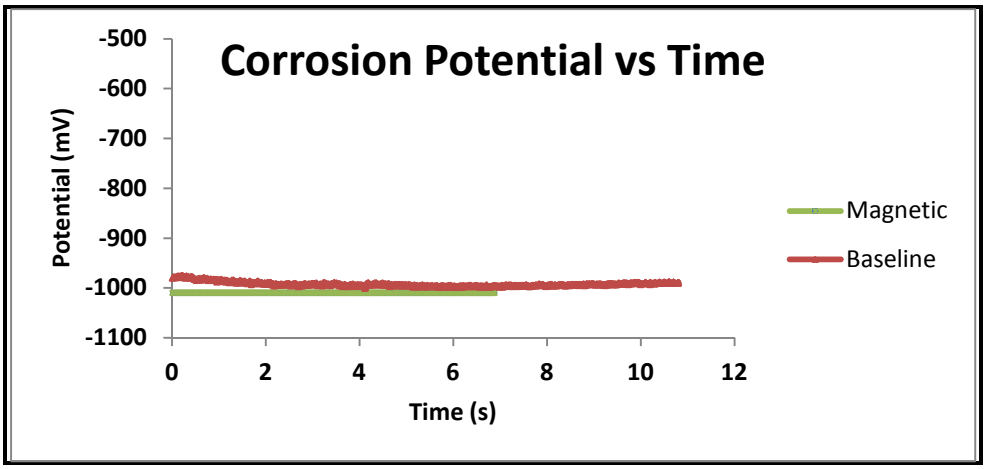

(a)

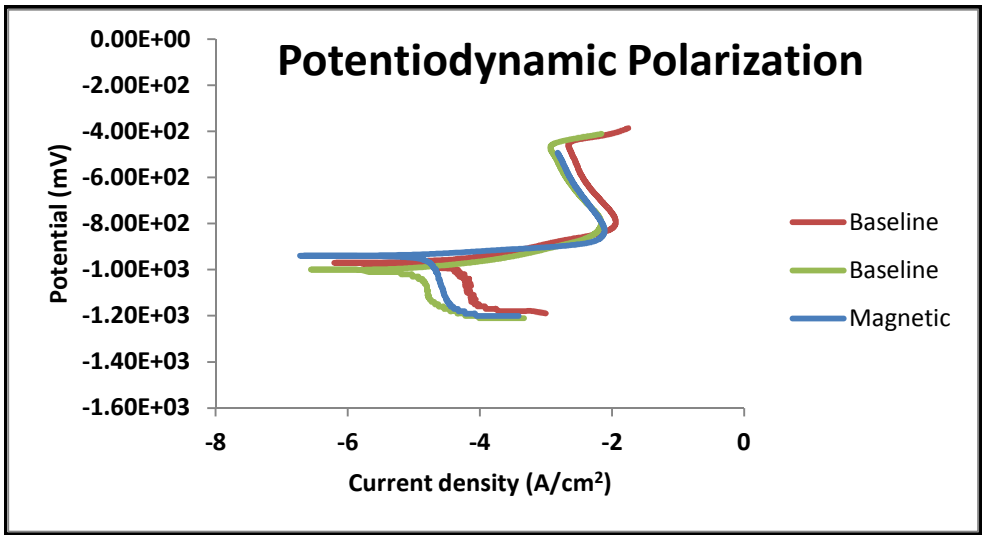

(b)

Figure 5-7: Comparison of results of (a) Corrosion potential Vs time measurement and (b) Potentiodynamic polarization curves of Zn in 3.5% NaCl, both without and with an external magnetic field

Table 5-4: Potentiodynamic polarization curves report of Zn in 3.5% NaCl solution with and without an external magnetic field

TYPE	Test 1	Test 2	Test 3
Magnetic field strength, B (T)	0 T	0 T	0.7 T
Corrosion Potential (mV)	-1003	-998	-978
Corrosion rate ($\mu A.cm^{-2}$)	31.60	30.19	28.18

5.3.1.5 Ti alloy (Ti-6Al-4V)

The corrosion potential vs time and potentiodynamic polarization test results obtained for Ti alloy (Ti-6Al-4V) in 3.5% NaCl, with and without the impact of an external magnetic field (baseline) are seen in Figures 5-8 (a) and (b), respectively. From Figure 5-8 (a) it can be seen that there is no effect of the magnetic field on the OCP. The corrosion potential reaches equilibrium at -278 mV and settles at a similar equilibrium potential of -273 mV when observed in 3.5% NaCl solution with and without the impact of a 0.7 T magnetic field, respectively. Also, from Figure 5-8 (b), which compares the potentiodynamic polarization curves, in both conditions, the anodic behavior of Ti alloy is seen. From the Tafel extrapolation method, the corrosion rate and corrosion potential was determined and shown in Table 5-5. Ti alloy has a very well-defined passive

region from -300 mV to 280 mV with constant current density of ~10^{-7} measured in 3.5% NaCl solution in both with and without impact of a magnetic field. The long passive range of Ti illustrates the highly stable nature of its passive oxide layer. Also, no effect of magnetic field is seen on the corrosion potential which is observed at -300 mV and corrosion rate of ~0.07 $\mu A/cm^2$.

Ti though has a negative standard metal/metal ion formation potential, its oxide layer has a very noble standard potential. Ti actively forms its oxide layer which is diffusion controlled. The effect of magnetic field driven forces are of much lower magnitude than the driving force for Ti oxide layer formation which confirms the previous studies on forces involved in the electrolyte. No effect of the external magnetic field of 0.7T is observed on Ti alloy as it is a non-magnetic material. Also, Ti^{4+} ions are diamagnetic in nature due to their paired electron configuration in their outer shell. It has zero unpaired electrons in its ionic state and hence is diamagnetic in nature. And hence, similar to highly passivating 304 SS, Ti alloy also has a very high passivating tendency and it being non-magnetic, has no effect of the magnetic field on its corrosion behavior in 3.5% NaCl solution.

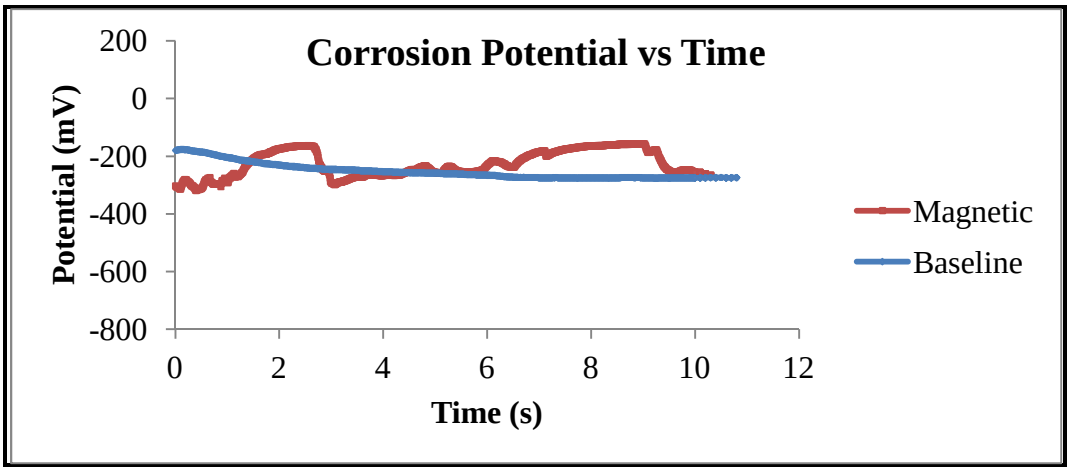

(a)

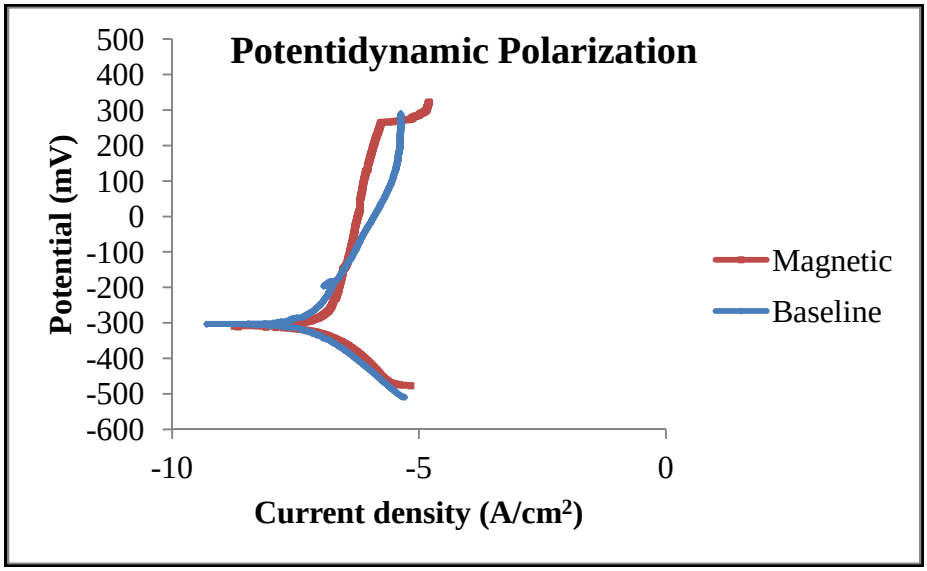

(b)

Figure 5-8: Comparison of results of (a) Corrosion potential Vs time measurement and (b) Potentiodynamic polarization curves of Ti alloy in 3.5% NaCl, both without and with an external magnetic field

Table 5-5: Potentiodynamic polarization curves report of Ti alloy in 3.5% NaCl solution with and without an external magnetic field

TYPE	**Test 1**	**Test 2**
Magnetic field strength, B (T)	0T	0T
Corrosion Potential (mV)	-300	-301
Corrosion rate ($\mu A.cm^{-2}$)	0.079	0.063

Chapter 6

CONCLUSIONS

Based on the electrochemical nature and magnetic properties of each material, the impact of an external magnetic field was determined in this research. Both ferromagnetic materials and diamagnetic materials have different response to an external force based on magneto-hydrodynamics and corrosion kinetics.

Few notable conclusions of the effect of a 0.7 T magnetic field on the corrosion behavior of selected materials in 3.5% NaCl solution were found to be as follows:

A. 304 SS: minimal impact on its corrosion rate and no effect on its corrosion potential. It enhances passivation of 304 SS.
B. 416 SS: increased its corrosion rate and reduced its corrosion potential (in the active direction). Oxygen being attracted to the regions of high magnetic flux, at the rim, causes increased pitting and overall increased dissolution.
C. 1018 steel: in the case of an active metal like 1018 steel, there is a cathodic shift of the corrosion potential because of increased dissolution. Fe^{2+} ions also being paramagnetic in nature are attracted to the rim, locally increasing the pH and also repels H^{+} ions which causes a slight lowering of corrosion rate, however, the overall rate remains high.

D. In the case of non-ferrous metals like Ti4Al6V and pure Zn, no effect on its corrosion behavior is seen because of its highly passive or active nature, respectively. The driving force involved in the electrochemical reaction itself is larger than other magnetic field influenced forces due to a magnetic field strength of 0.7 T.

Magnetic field of 0.7 T therefore affects ferromagnetic materials by attracting oxygen to the surface and increasing the anodic current and promoting either passivation or dissolution based on the type of material. The electronic configuration of the outer shell of ions that dissolve in the electrolyte also plays a role in affecting the corrosion kinetics.

References

1. Jones D.A, (1996). Principles and Prevention of Corrosion. Upper Saddle River, New Jersey. Prentice Hall. ISBN-13:3599930.

2. US Navy Research on Corrosion http://www.navsea.navy.mil/teamships/Sailing_Directions/Corrosion_Prevention.aspx

3. T.Z. Fahidy, J. Appl. Electrochem. 13 (1983) 553.

4. O. Aaboubi, J.P. Chopart, J. Douglade, A. Olivier, C. Gabrielli, B. Tribollet, J. Electrochem. Soc. 137 (1990) 1796.

5. R.A. Tacken, L.J.J. Janssen, J. Appl. Electrochem. 25 (1995) 1.

6. T.Z. Fahidy, The effect of magnetic fields on electrochemical process, in: B.E. Convey, J.O'.M. Bockris, R.E.White (Eds.), Modern Aspects of Electrochemistry, Kluwer Academic/Plenum Press, New York, 1999, pp.333–353.

7. E.J. Kelly, J. Electrochem. Soc. 1214 (1977) 987.

8. R. Aogaki, T. Negishi, M. Yamato, E. Ito, I. Mogi, Phys. B: Condens. Matter 201 (1994) 611.

9. Z.P. Lu, J.M. Chen, J. Chinese Soc. Corros. Protect. 15 (1995) 303.

10. J.H. Lee, S.R. Ragsdale, X.P. Gao, H.S. White, J. Electroanal. Chem. 422 (1997) 169.

11. G. Hinds, J.M.D. Coey, M.E.G. Lyons, Electrochem. Commun. 3 (2001) 215.

12. THE ELECTROCHEMISTRY OF CORROSION, Edited by Gareth Hinds from the original work of J G N Thomas

13. G.A. Cragnolinio, (2008). Corrosion Fundamentals and Characterization Technique, Woodhead Publishing Limited, 80 High Street Sawston CB22 3HJ UK. ISBN 13:9781845691875.

14. P. Lorbeer, W.J. Lorenz, The kinetics of iron dissolution and passivation in solutions containing oxygen, Electrochim. Acta 25 (1979) 375–381.

15. A.A. El Miligy, D. Geana, W.J. Lorenz, A theoretical treatment of the kinetics of iron dissolution and passivation, Electrochim. Acta 20 (1974) 273–281.

16. J. Bessone, L. Karakaya, P. Lorbeer, W.J. Lorenz, The kinetics of iron dissolution and passivation, Electrochim. Acta 22 (1976) 1147–1154.

17. J.O'M. Bockris, D. Drazic, A.R. Despic, The electrode kinetics of the deposition and dissolution of iron, Electrochim. Acta 4 (1961) 325–361.

18. H. Schweickert, W.J. Lorenz, H. Friedburg, Impedance measurements of the anodic iron dissolution, J. Electrochem. Soc. 127 (1980) 1693–1701.

19. T.Z. Fahidy, J. Appl. Electrochem. 13 (1984) 553–563.

20. O. Aaboubi, J.P. Chopart, J. Douglade, A. Olivier, C. Gabrielli, B.Tribollet, J. Electrochem. Soc. 137 (1990) 1796–1804.

21. T.Z. Fahidy, The effect of magnetic fields on electrochemical process, in: B.E. Conwey, J.O'.M. Bockris, R.E. White (Eds.), Modern Aspects of Electrochemistry, Kluwer, Academic/Plenum Press, New York, 1999, pp. 333–353.

22. O. Devos, O. Aaboubi, J.P. Chopart, A. Olivier, C. Gabrielli, B. Tribollet, J. Phys. Chem. A 104 (2000) 1544–1548.

23. S. Koehler, A. Bund, J. Phys. Chem. B 110 (2006) 1485–1489.

24. M. Waskaas, Y.I. Kharkats, J. Phys. Chem. B 103 (1999) 4876–4883.

25. M. Waskaas, Y.I. Kharkats, J. Electroanal. Chem. 502 (2001) 51–57.

26. F.M.F. Rhen, G. Hinds, J.M.D. Coey, Electrochem. Commun. 6 (2004) 413–416.

27. F.M.F. Rhen, D. Fernandez, G. Hinds, J.M.D. Coey, J. Electrochem.Soc. 153 (2006) J1-J7.

28. F.M.F. Rhen, J.M.D. Coey, J. Phys. Chem. C 111 (2007) 3412–3416.

29. E.J. Kelly, J. Electrochem. Soc. 123 (1976) C246.

30. S. Yamanaka, R. Aogaki, M. Yamato, E. Ito, I. Mogi, Science Reports of the Research Institutes Tohoku University Series a- Physics Chemistry and Metallurgy 38 (1993) 399–405.

31. R. Aogaki, T. Negishi, M. Yamato, E. Ito, I. Mogi, Physica B 201 (1994) 611–615.

32. J.H. Lee, S.R. Ragsdale, X.P. Gao, H.S. White, J. Electroanal. Chem. 422 (1997) 169-177.

33. S.R. Ragsdale, K.M. Grant, H.S. White, J. Am. Chem. Soc. 120 (1998) 13461–13468.

34. K.M. Grant, J.W. Hemmert, H.S. White, J. Electroanal. Chem. 500 (2001) 95–99.

35. Z.P. Lu, J.M. Chen, J. Chin Soc. Corros. Protect. 15 (1995) 303–307.

36. J.M. Chen, Z.P. Lu, J. Chin. Soc. Corros. Protect. 17 (1997) 276–280.

37. Z.H. Gu, A. Olivier, T.Z. Fahidy, Electrochim. Acta 35 (1990) 933– 943.

38. Z.P. Lu, J.M. Chen, J. Chin. Soc. Corros. Protect. 17 (1997) 203–209.

39. K. Shinohara, K. Hashimoto, R. Aogaki, Chem. Lett. (2002) 738– 739.

40. Z.P. Lu, D.L. Huang, W. Yang, J. Congleton, Corros. Sci. 45 (2003) 2233–2249.

41. Z.P. Lu, D.L. Huang, W. Yang, Corros. Sci. 47 (2005) 1471–1492.

42. Z.P. Lu, C.B. Huang, D.L. Huang, W. Yang, Corros. Sci. 48 (2006) 3049–3077.

43. J. Chopart, J. Douglade, P. Fricoteaux, A. Olivier, Electrochim. Acta 36 (1991) 459. C.-C. Lee, T.-C. Chou, Electrochim. Acta 40 (1995) 965.

44. K. Shinohara, R. Aogaki, Electrochemistry 67 (1999) 1261.

45. G. Hinds, J.M.D. Coey, M.E.G. Lyons, J. Appl. Phys. 83 (1998) 6447.

46. O. Aaboubi, J.O. Chopart, J. Douglade, A. Olivier, C. Gabrielli, B. Tribollet, J. Electrochem. Soc. 137 (1990) 1796.

47. K. Kim, T.Z. Fahidi, J. Electrochem. Soc. 142 (1995) 4196.

48. J. Lee, S.R. Ragsdale, X. Gao, H.S. White, J. Electroanal. Chem. 422 (1997) 169.

49. S. Mori, K. Satoh, A. Tanimoto, Electrochim. Acta 39 (1994) 2789.

50. V. Novinski, Electrochim. Acta 42 (1997) 251.

51. A. Chiba, N. Tanaka, S. Ueno, T. Ogawa, Corros. Eng. 41 (1992) 333.

52. A. Chiba, T. Ogawa, Corros. Eng. 38 (1989) 557.

53. A. Chiba, K. Kawazu, O. Nakano, T. Tamura, S.Yoshihara, E. Sato, Corros. Sci. 36 (1994) 539.

54. A. Rucinskiene, G. Biculsius, L. Gudaviciute, E. Juzeliunas, Electrochem. Commun. 4 (2002) 86.

55. E.J. Kelly, J. Electrochem. Soc. 124 (1977) 987.

56. R.N. O'Brien, K.S.V. Santhanam, J. Appl. Electrochem. 27 (1997) 573.

57. Y. Yang, K.M. Grant, H.S. White, S. Chen, Langmuir 19 (2003) 9446.

58. K.L. Rabah, J.-P. Chopart, H. Schloerb, S. Saulnier, O. Aaboubi, M. Uhlemann, D. Elmi, J. Amblard, J. Electroanal. Chem. 571 (2004) 85.

59. M. Uhlemann, A. Krause, J.-P. Chopart, A. Gebert, J. Electrochem.Soc. 152 (2005) 817.

60. A. Bund, H.H. Kuehnlein, J. Phys. Chem. B 109 (2005) 19845.

61. N. Leventis, A. Dass, J. Am. Chem. Soc. 127 (2005) 4988.

62. J.M.D. Coey, F.M.F. Rhen, P. Dunne, S. McMurry, J. Solid State Electrochem. 11 (2007) 711.

63. N. Leventis, A. Dass, N. Chandrasekaran, J. Solid State Electrochem.11 (2007) 727.

64. A. Krause, J. Koza, A. Ispas, M. Uhlemann, A. Gebert, A. Bund, Electrochimica Acta 52 (2007) 6338.

65. R. Sueptitz, K. Tschulik, M. Uhlemann, L. Schultz, A. Gebert, Corrosion Science 53 (2011) 3222- 3230.

66. Tom Weier, Kerstin Eckert, Sascha Muhlenhoff, Christian Cierpka, Andreas Bund, Margitta Uhlemann, Electrochemistry Communications 9 (2007) 2479-2483.

67. R. O'Brien, K. Santhanam, J. Electrochem. Soc. 129 (1982) 1266.

68. H. Richard, M. Raffel, Meas. Sci. Technol. 12 (2001) 1576.

69. Y.C. Tang, A.J. Davenport, J. Electrochem. Soc. 154 (2007) C362.

70. Z. Lu, J.-M. Chen, Br. Corros. J. 45 (3) (2000) 224.

71. Z.P. Lu, T. Shoji, W. Yang, Anomalous surface morphology of iron generated after anodic dissolution under magnetic fields, Corros. Sci. 52 (2010) 2680–2686.

72. R Sueptitz, J. Koza, M. Uhlemann, A. Gebert, L. Schultz, Electrochimica Acta 54 (2009) 2229-2233.

73. Y.C. Tang, M. Gonzalez-Torreira, S. Yang, A.J. Davenport, JCSE 6 (2007) 46.

74. C. Muller, M. Sarret, M. Benballa, Electrochim. Acta 46 (18) (2001) 2811.

75. J.B. Bajat, Z. Kacarevie-Popovie, V.B. Miskovie, M.D. Maksimovie, Prog. Org. Coat. 39 (2000) 127.

76. R. Ramanauskas, L. Muleshkova, L. Maldonado, P. Dobrovolskis, Corros. Sci. 40 (1998) 401.

77. R. Fratesi, G. Rovinti, Surf. Coat. Technol. 82 (1996) 158.

78. Z. Zhou, T.J. O'Keefe, Surf. Coat. Technol. 96 (1997) 191.

79. M.R. Kalantary, G.D. Wilcox, D.R. Gabe, Electrochim. Acta 40 (1995) 1609.

80. R. Ramanauskas, Appl. Surf. Sci. 153 (1999) 53.

81. Z. Wu, L. Fedrizzi, P.L. Bonora, Surf. Coat. Technol. 85 (1996) 170.

82. CEE Recommendation (Directive du Conseil de la Communaute Europeenne)n◦ 91/338/CEE, 1991.

83. M. Gavrila, J.P. Millet, H. Mazille, D. Marchandise, J.M. Cuntz, Surf. Coat. Technol. 123 (2000) 164–172.

84. K.R. Baldwin, M.J. Robinson, C.G.E. Smith, Corros. Sci. 36 (1994) 1515.

85. R. Albalat, E. Gomez, C. Muller, J. Pregonas, M. Sarret, E. Valles, J. Appl. Electrochem. 21 (1991) 44.

86. K.H. Lee, J. Yoo, J. Ko, H. Chung, D. Chang, et al., Phys. C 372 (2002) 866.

87. A. Rucinskiene, G. Bikulcius, L. Gudavicuite, E. Juzelias, Electrochem. Commun.4 (2002) 86.

88. H.R. Khan, K. Petrikowski, Mater. Sci. Forum 373 (2001).

89. C. O'Reilly, G. Hinds, J.M.D. Coey, J. Electrochem. Soc. 148 (2001) C674.

90. T.Z. Fahidy, Prog. Surf. Sci. 68 (2001) 155.

91. S. Bodea, L. Vignon, R. Ballou, P. Molho, Phys. Rev. Lett. 83 (1999) 267.

92. O. Devos, A. Olivier, J.P. Chopart, O. Aaboubi, G. Maurin, J. Electrochem. Soc. 145 (1998) 401.

93. D.Y. Li, J. Appl. Electrochim. Acta 42 (1997) 37.

94. A. Chiba, T. Ogawa, T. Yamshita, Surf. Coat. Technol. 34 (1988) 455.

95. R. Aogaki, K. Fueki, T. Makaido, Denki Kagaku 44 (1976) 89.

96. L. Yang, J. Electrochem. Sci. 101 (1954) 456.

97. J.C. Shannon, Z.H. Gu, Z.T. Fahidy, J. Electrochem. Soc. 145 (1998) L314.

98. A. Krause, C. Hamann, M. Uhlemann, A. Gebert, L. Schultz, J. Magn. Magn. Mater. 290 (2005) 261.

99. A. Krause, M. Uhlemann, A. Gebert, L. Schultz, Electrochim. Acta 49 (2004) 4127.

100. S. Chouchane, A. Levesque, P. Zabinski, R. Rehamnia, J.-P. Chopart, Journal of Alloys and Compounds 506 (2010) 575-580.

101. P. Linhardt, G. Ball, E. Schlemmer, Corrosion Science 47 (2005) 1599-1603

102. Zhanpeng Lu, Wu Yang, Corrosion Science 50 (2005) 510-522.

Biographical Information

Soundarya Pondichery was born in Bangalore, India. She received her bachelor degree in Materials and Metallurgical Engineering from Mahatma Gandhi Institute of Technology (J.N.T.U affiliated) Hyderabad, India in 2012. Her undergrad project was on a Study on the Formation of Microdroplets during Metal Ion Etching in CAPVD. During her undergrad she worked as a student researcher in Advanced Research Centre International at Hyderabad, India. Her work involved the study on the defects in thin film coatings by Cathodic Arc Vapor Deposition technique and material characterization using Scanning Electron Microscope and other characterization tools.

In January 2013 she began her masters in Material Science and Engineering program in the University of Texas at Arlington. She started her research project under Dr. E.I. Meletis from May 2013 in the *Surface and Nano Engineering Laboratory* on the effect of an external magnetic field on the corrosion behavior of materials in 3.5% sodium chloride solution involving a permanent magnet of 0.7 T and different types of metals.